GEOMORPHIC RESPONSE OF FALL RIVER TO THE 2013 FLOOD

by

MARK SCHUTTE
B.S., University of Cincinnati, 2013

A thesis submitted to the
Faculty of the Graduate School of the
University of Colorado in partial fulfillment
of the requirement for the degree of
Master of Science
Department of Civil Engineering
2015

This thesis entitled:
Geomorphic response of Fall River to the 2013 flood
written by Mark Paul Schutte
has been approved for the Department of Civil Engineering

John Pitlick

Roseanna Neupauer

Hari Rajaram

Date _____

The final copy of this thesis has been examined by the signatories, and we find that both the content and the form meet acceptable presentation standards of scholarly work in the above mentioned discipline.

Schutte, Mark (M.S. Hydrology, Water Resource & Environmental Fluid Mechanics)
Geomorphic Response of Fall River to the 2013 Flood
Thesis directed by Professor John Pitlick

In Rocky Mountain National Park, the 2013 flood destabilized segments of Roaring River and deposited an unusually large amount of sand- and gravel-sized sediment near the confluence with Fall River. We initiated field studies of these two rivers in May 2014 to investigate the geomorphic response of Fall River to an increase in sediment supply. Measurements of water discharge and bed load were taken from May through August at three different locations to capture variations in sediment transport rates.

Peak transport rates coincided with the peak discharge at the upstream sampling site (FR 1), but lagged behind the peak in discharge at the lower site (FR 2) by about three weeks, which is consistent with diffusive movement of sediment as observed in earlier studies. On average, 2014 transport rates were 0.015 kg/m/s and 0.035 kg/m/s at FR-1 and FR-2, respectively. Bankfull Shields stress calculations showed a nearly constant value across the study area, about 0.056. A combination of changing slope, depth, and grain size throughout the study area resulted in the same estimated value of reference Shields stress at each site, 0.028.

Annual sediment loads estimated at each site, as well as erosion and deposition tracked by comparing cross sections measurements, both indicate a majority of the sediment deposited by the flood was eroded and transported out of the Fall River channel in 2014. Annual sediment loads were estimated from discharge- and shear stress-based empirical relations and a time series of discharge scaled to the continuous discharge of the Big Thompson River from a nearby USGS gage in Moraine Park. Annual loads estimated at FR 1 and FR 2 were about 3,000 Mg and 4,600 Mg, respectively. Relative to the estimates following the 1982 Lawn Lake flood, annual loads

were lower than the three years immediately following the flood, but comparable to the loads estimated four to five years after the flood.

Analysis of the results of the field data collected indicate that Fall River experienced some erosion in 2014, transporting sediment which had been stored in its channel from the flood. Fall River was primarily able to accommodate the increase in sediment supply by adjusting its bed texture, and secondarily due well-vegetated banks which prevented channel widening. Annual sediment loads estimated from all approaches indicate that Fall River was able to transport a majority of the sediment supplied to it in 2014.

Acknowledgements

There are many people who I must thank for their support of my work: first and foremost, my professor, Dr. John Pitlick. John took me under his guidance and taught me everything I know about fluvial geomorphology. John's technical knowledge and good humor made the completion of this thesis that much easier. This work would not have been possible without his help.

Field work is no one-man job, and I could not have collected the information needed without the help of a few good people. Luca Rossi was my coworker, peer, and friend throughout our field work in Rocky Mountain National Park. Luca and I walked side by side throughout Fall River, and there is no one else with which I would have wanted to share that summer and experience. Liz Houle, a close friend and peer at CU, also helped me on several days in the field.

While I may no longer live near them, my parents, Larry and Kate Schutte, have been a constant pillar of support and encouragement. Thank you to the two people who taught me to work hard, to check my work, and always give my best effort.

Finally, I must thank the generous supporters of this research study. Thank you to Rocky Mountain National Park for their financial support of this study. I would like to specifically thank Ben Bobowski and Paul McLaughlin for their direct involvement and assistance in my work in Rocky Mountain National Park.

Contents

Chapter I: Introduction

Significant events, such as floods, often lead to increases in the sediment supply to rivers, which can potentially cause changes in channel morphology. For a given hydrologic regimen, a river can effectively respond to this imposed change in sediment supply in different ways, which are constrained by the geomorphic history and boundary conditions of the river. In a general sense, *Schumm* [1969] proposed how a river will change physically in response to altered flow, Q_w, and sediment supply, Q_t:

$$Q_w^+, Q_t^+ \cong \frac{W^+ L^+ F^+}{P^-} S^{\pm} H^{\pm}$$

$$Q_w^-, Q_t^- \cong \frac{W^- L^- F^-}{P^+} S^{\pm} H^{\pm}$$

$$Q_w^+, Q_t^- \cong \frac{H^+ P^+}{S^- F^-} W^{\pm} L^{\pm}$$

$$Q_w^-, Q_t^+ \cong \frac{H^- P^-}{S^+ F^+} W^{\pm} L^{\pm}$$

where *W* is width, *L* is meander wavelength, *F* is width-depth ratio, *P* is sinuosity, *S* is channel gradient, and *H* is depth.

While Schumm's equations provide a context for the possible adjustments a river can make, they do not explain all the complexities affecting sediment transport. The physical characteristics of rivers adjust on different time scales in response to changes in hydrology and sediment supply, which operate on their own time scales. Gradient is a very effective means of transporting sediment, but requires a significant amount of time to change. Over shorter timescales, increased sediment supply from a single significant event can be accommodated by changes in depth, and even more immediately, width [*Pizzuto*, 1992]. However, the most

immediate response to increased sediment supply tends to be an adjustment of bed surface texture. This is not apparent in Schumm's equations above, because they do not address the effects of boundary conditions in a river, like bank stability and bed surface texture. *Eaton and Church* [2009] showed that non-erodible banks constrain the adjustments a river will make; rivers adjust bed surface texture to accommodate two- to four-fold increases in sediment supply, instead of their channel geometry. For a river to withstand physical changes from increased sediment supply, sediment must be transported through the channel quickly. The river's geomorphic response can therefore be quantified by measuring changes in channel and bed material properties reflecting the passage of sediment through the affected reaches.

Researchers have spent a significant amount of time investigating how the combination of water and sediment supply affect a river's physical characteristics, and, consequently its capacity to transport sediment. Many of these relations have been demonstrated in lab-scale experiments. Where banks are non-cohesive, flume studies suggest that channels seem to adjust either their average gradient, by means of sinuosity [*Eaton and Church*, 2004], or their bankfull width by means of bank erosion [*Pitlick et al.,* 2013]. Several field studies have contributed to the understanding of channel change, as well. *Pizzuto* [1994] observed that net bank erosion or deposition varied with discharge on the Powder River in Montana. Along the Cimarron River in Kansas, *Schumm and Lichty* [1963] found channel width adjustment to be the primary means of morphologic modification over decades of climatologic changes. Channel width typically increased due to significant floods, and narrowed when years of above-average precipitation and moderate peak discharges encouraged vegetation growth and bank stabilization.

Through field work and flume studies, others have investigated the relations between changes in hydrology or sediment supply and morphologic adjustments of the river's bed surface

texture. In experiments using a range sediment supplies to a flume, results indicate that the bed surface texture fined as sediment supply increased; subsequently, sediment transport rates increased due to bed surface texture's influence on transport [*Dietrich et al.*, 1989; *Kuhnle*, 1989]. *Wilcock et al.* [2001] found that when sediment supply was recirculated through a flume, a coarse bed surface layer was retained, even as discharge and sediment load increased. The median surface grain size varied with sand content of the sediment feed, but did not adjust to increases in discharge. Further studies confirm this result, showing that sediment supply, primarily, and the shape of the hydrograph, secondarily, influence the extent of armoring on the bed surface [*Hassan et al.*, 2006]. While these studies have improved our knowledge of a river's response to changing water and sediment input, more data are required to refine these concepts. Present studies seek to further the understanding of a gravel-bed river's response to an increased sediment supply following a significant event by investigating Fall River's primary physical adjustment to the 2013 flood.

Influence of Significant Events and Historic Conditions

Significant events, like floods, can quickly inundate river channels causing incision of the bed in upstream reaches and massive aggradation where gradient declines and its valley widens. The resulting impacts of floods on rivers are quite variable depending on flow and sediment supply, a result which has been observed in nature many times. Glacial-lake outburst floods studied in the Mount Everest region of Nepal resulted in significant erosion and transport of sediment, due to peak discharges 7 to 60 times the normal flood and an abundance of sediment supplied from a breached moraine [*Cenderelli and Wohl*, 2001; 2003]. Results from this study also showed that geomorphic change was most significant at upstream portions nearest the

breach, and the impacts of the flood-supplied sediment transport lessened as stream power decreased in downstream reaches. *Lapointe et al.* [1998] observed similar patterns of erosion and deposition in their analysis of the Ha! Ha! River's response to the 1996 flood in the Saguenay region of Quebec. There, two large-scale avulsions in upstream portions of the river transported 6,000,000 cubic meters of sediment, resulting in extensive sedimentation of downstream reaches. In Switzerland, three days of heavy rainfall in 2005 produced high, sustained flood flows in mountain rivers along the northern side of the Alps [*Rickenmann*, 2010]. In these rivers, sediment transport ranged from 5,000 to 225,000 cubic meters due to the flood events. In Rocky Mountain National Park (RMNP), the effects of significant events have been studied on several rivers. In 2003 a breach in the Grand Ditch in RMNP caused severe erosion of Lulu Creek, significantly increasing sediment supply to the Colorado River. Between 2004 and 2010, *Rathburn et al.* [2013] measured sediment transport rates on the Colorado River as high as 1.0 kg/s. On the eastern slopes of RMNP, the Lawn Lake Flood, as it was called, resulted in peak discharges eight times greater than the 500-year flood for Fall River [*Jarrett and Costa*, 1986]. Soil destabilized in Roaring River during the flood inundated the Fall River channel in 1983, where above-average discharges caused deposition throughout Fall River, with significant aggradation in lower gradient reaches downstream [*Pitlick*, 1993]. The direct impact of significant events can be severe, but events cause further morphologic adjustment by increasing sediment supply.

The impact of significant events on sediment supply, and subsequently the morphologic response of a river, is influenced by the climatological and physical conditions of a river. Studies suggest that infrequent, significant events can result in significant channel change. *Costa and O'Connor* [1995] found that the extent of the impact on the river depends on the time

scale of the disturbance event. The response of the river, for a given event, is then tempered by the climate and physical conditions surrounding the river. A study of streams affected by flash flooding in Central Texas, indicates that climate appears to influence the potential for catastrophic channel response to floods only to the extent permitted by physical controls, such as rock type, drainage density, vegetation cover, and hillslope steepness [*Baker*, 1977]. *Lisle* [1981] found that streams in northern California and southern Oregon experienced sustained aggradation due to large floods for more than 20 years. The rivers were unable to recover quickly to pre-flood levels as a direct result of highly erosive terrain and heavy seasonal rainfall, which constantly supplied more sediment.

Sediment Transport Estimation

Estimates of sediment transport following a significant event provide engineers and geomorphologists with a quantifiable characterization of the geomorphic response of a river. The most accurate method of quantifying sediment transport would require constant sampling; since this is not possible or practical, researchers use bed load transport functions calibrated to measured data to estimate sediment transport when sampling did not occur. Sediment transport is typically estimated through a relation to the discharge of the river, and not surprisingly, sediment transport generally increases as discharge increases. However, accuracy of the estimates of sediment load can be difficult to achieve since this relation is highly non-linear, and transport is influenced by more than discharge alone. To utilize the information embedded in shear stress, a significant amount of effort has been spent creating accurate bed load transport functions capable of capturing the various morphologic responses that a wide range of rivers exhibit. Arguably the

most notable, the Meyer-Peter Müller formula [*Meyer-Peter and Müller*, 1948] relates excess Shields stress to transport:

$$q_s^* = 8(\tau^* - \tau_c^*)^{\frac{3}{2}}$$

where q_s* is Einstein's dimensionless transport parameter, τ* is Shields stress, and τ_c* is critical Shields stress.

More recently, sediment transport rates have been related to a ratio of shear stresses, which will be the primary approach of this study. This two-part function is based on transport functions developed by *Parker* [1979; 1990]. The transport function can be written as

$$W^* = \begin{cases} 11.2\left(1 - \dfrac{0.853}{\phi}\right)^{4.5} & \phi \geq 0.853 \\ 0.002\phi^{14.2} & \phi < 0.853 \end{cases}$$

where W* is a dimensionless transport rate, and ϕ, the transport stage, is equal to τ^*/τ_r^*, the ratio of available Shields stress to the reference Shields stress, a corollary of the critical Shields stress.

Using sediment transport functions to accurately estimate transport in rivers has value in a range of applications. *Abderrezzak* [2011] investigated the utility of a variety of sediment transport functions in modelling dam breaks. *Cui* [2000] created a 1D model based on Parker's bed load equations to predict sediment transport for different dam removal scenarios. *Erwin* [2011] was able to quantify the effects of dam impoundment on sediment transport for the Snake River using a nearly identical approach to the present study, finding that flow regulation has actually aided the river by decreasing sediment transport rates from what would occur naturally. *Lewicki et al.* [2007] created a model using Parker's transport equations to investigate the impacts of land use on transport. In the Williams Fork River in Colorado, *Segura and Pitlick* [2015] used Parker's transport equations to study variations in sediment transport and its effects on benthic organisms in a snowmelt-dominated watershed. Field studies such as these aid in

strengthening the connection between transport relations and the reality of their application, by evaluating the validity of their use.

2013 and 1982 Floods

The present study focuses on the near-term response of Fall River in RMNP to an unusual flood spawned by intense rainfall in Sept. 2013. From September 9 to 15, 190 mm of rain fell over Fall River in Horseshoe Park, a low gradient glacial valley where the study was conducted, resulting in significant flooding in the range of the 100-year flood [*Yochum and Moore*, 2013]. Based on a reconstruction of the flood in HEC-RAS, the flood discharge through Fall River was around 20 cms. Sediment supplied to Fall River in 2013 was increased by a flood in 1982, when an old earthen dam structure on Lawn Lake failed catastrophically. Large amounts of sand- and gravel-sized sediment were routed through Roaring River and deposited in an alluvial fan at the confluence with Fall River in Horseshoe Park. During the thirty years following the Lawn Lake flood, many steep segments of Roaring River did not recover, and the September 2013 flood easily reworked this destabilized sediment for transport into and through Fall River. Though smaller in magnitude, the initial effects of the 2013 flood closely resembled that of the dam break in 1982. In addition, a buildup of boulder-sized sediment at the head of the alluvial fan in Horseshoe Park, caused a shift in Roaring River's channel about 100 meters west, washing out Old Fall River Road. New sediment was deposited on top of the original alluvial fan at the confluence with Fall River, and along the Fall River channel throughout Horseshoe Park. While the flood effects were somewhat diminished by the open, flat area of this alpine valley, the flood continued downstream along Fall River, growing in size and causing severe damage in Estes Park.

Objectives

1. Determine the geomorphic impact of the sediment supplied by the 2013 flood on Fall River with respect to the change in its physical characteristics.
2. Accurately estimate sediment loads in Fall River for 2014.
3. Compare results of annual sediment load calculations for discharge- and shear stress-based empirical transport relations.
4. Compare sediment loads in 2014 to values from 1983 to 1987 to understand the effects of the 2013 flood in an historical context.
5. Assess the potential for future geomorphic change based on the instability of sediment in Roaring River.

Chapter II: Study Area and Methods

Study Area

This study focuses on a five kilometer segment of Fall River located within Horseshoe Park in Rocky Mountain National Park, Colorado (Figure 2.1). Horseshoe Park has been formed over long periods of time by glacial advance and retreat, giving the valley a characteristic U-shape and relatively low gradient. Bedrock in the headwaters of the Fall River basin consists of Precambrian gneiss, granite, and schist, while most of the area around Horseshoe Park is underlain by glacial deposits [*Cole and Braddock*, 2009].

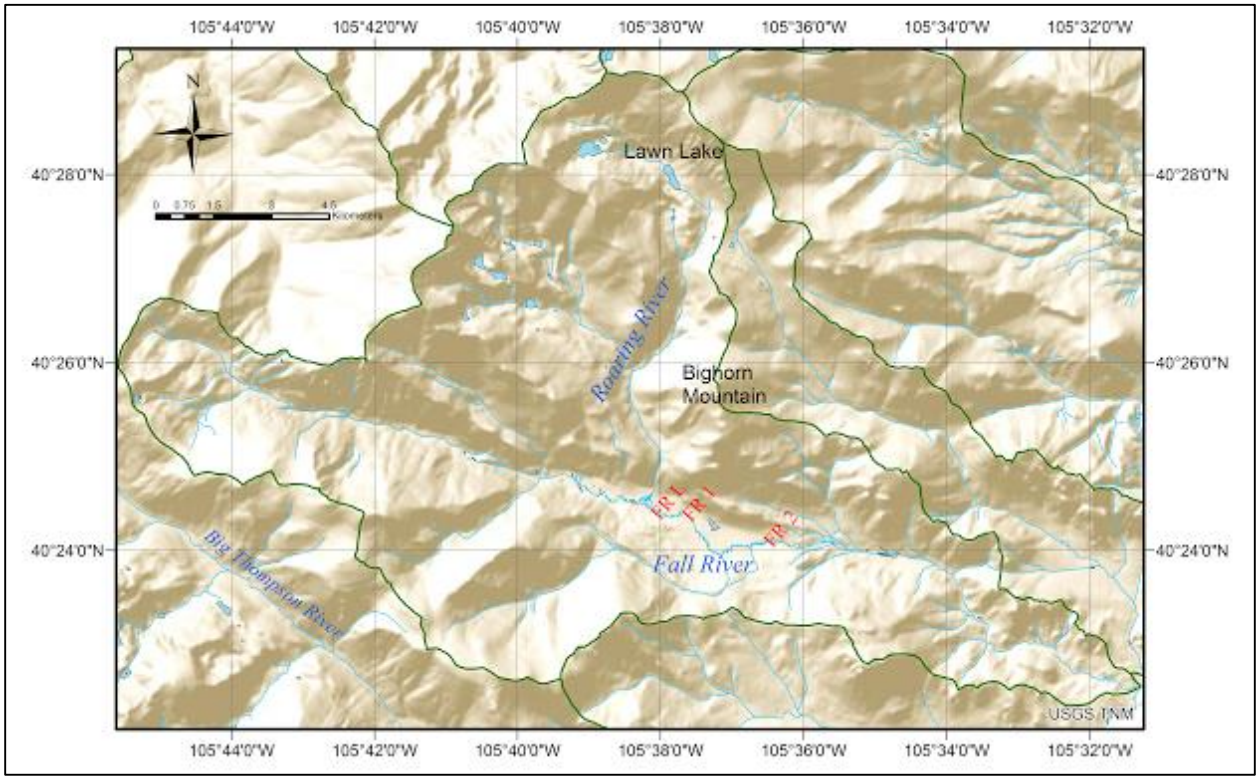

Figure 2.1. Site map showing entire Fall River watershed with sampling sites marked to identify study area.

Annual precipitation in the study area averages between 800 and 900 mm [*NRCS-NWCC*, 2015], with most of the precipitation falling as snow between the months of October and May. A majority of runoff occurs in the three-month period of snowmelt from May through July, and

overall runoff averages about 50% of annual precipitation [*NRCS-NWCC*, 2015]. Consequently, peak discharges in alpine basins of the Colorado Front Range, are generated almost exclusively by snowmelt, and annual flood discharges rarely exceed the mean annual flood by more than a factor of two [*Pitlick*, 1994].

As Fall River flows through Horseshoe Park, it can be defined by two general segments (Figure 2.2; Figure 2.3). The first segment extends from the confluence with Roaring River to the Highway 34 bridge, about 1600 m downstream. In this region the channel is relatively straight and the average gradient is 0.0052. The second segment, below the Highway 34 bridge to the outlet of Horseshoe Park, covers about the same distance as the first segment, but here the channel is highly sinuous and the gradient is much lower, 0.0025.

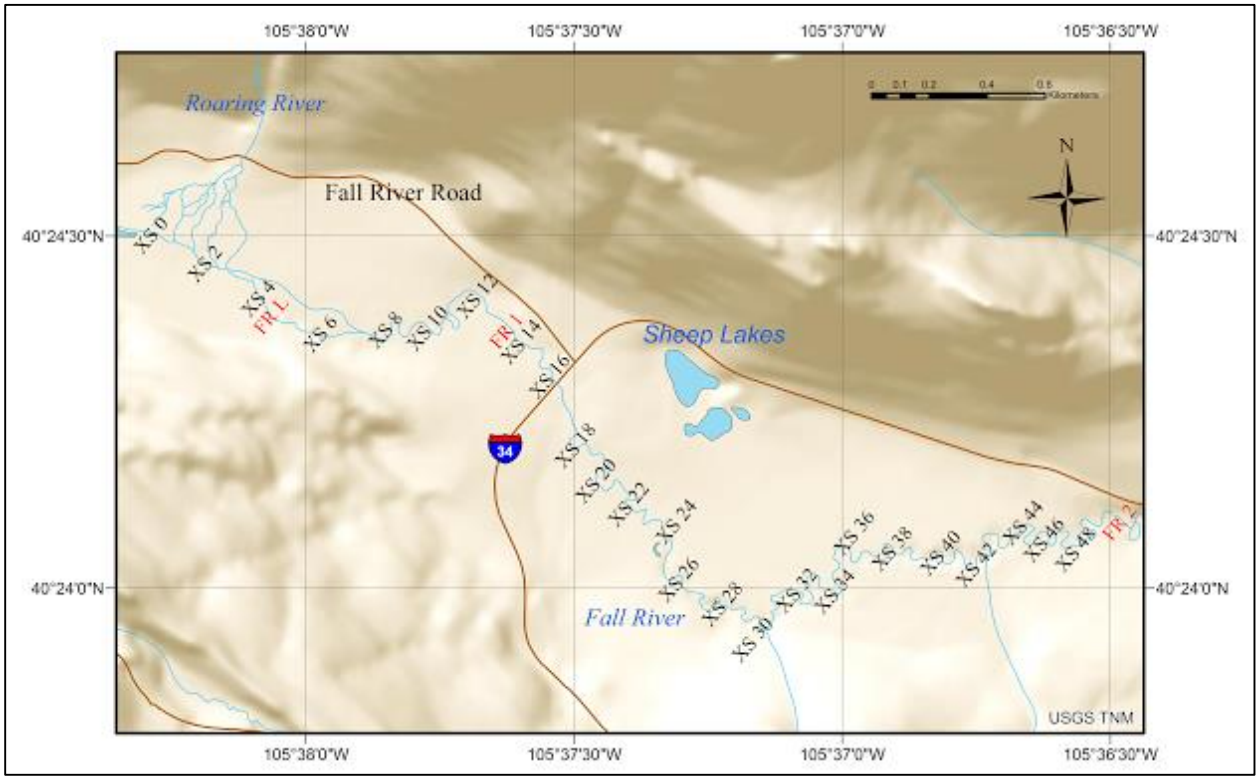

Figure 2.2. Detailed map showing extent of study area from the confluence with Roaring River to Fall River's exit from Horseshoe Park. Every other cross section is shown for clarity, including sampling sites marked in red.

Figure 2.3. Characteristic regions of Fall River. a) Downstream view of Fall River at XS 7, showing higher gradient and straighter channel typical of upper region. b) Overview of downstream portion of Fall River exhibiting high sinuosity, heavy vegetation on both banks, and lower gradient.

Methods

Measurements of discharge and bed load transport were taken at three sites designated FR L, FR 1, and FR 2 (Figure 2.1; Figure 2.2). Measurements were taken throughout the period of snowmelt runoff, beginning in mid-May, ending in mid-August, 2014. These sites were chosen based on site characteristics (e.g. uniform width, depth, and slope) and ease of access for the entire field season. Basic information for each site is summarized in the following table.

Table 2.1. Sampling Site Characteristics

Site	Drainage Area (km^2)	Slope (-)	Bankfull Width (m)	Bankfull Depth (m)	Surface Grain Size (mm)	Subsurface Grain Size (mm)
FR L	65.5	0.0056	10.3	0.48	43	14
FR 1	66	0.0042	8.2 / 14.0	0.62 / 0.5	21	3
FR 2	81	0.0012	7.6	0.9	8	1

FR L

The furthest upstream site, FR L, is located about 500 meters downstream of the confluence with Roaring River (Figure 2.2). Samples were collected near the middle of a relatively straight reach measuring 100 meters in length. The north bank of the channel consists of a coarse gravelly lateral bar that appears to have been deposited during the 2013 flood. The south bank consists of deposits from the Lawn Lake flood that are now vegetated and thus relatively stable. The median grain size (D_{50}) of the bed surface layer at this site is roughly 43 mm (Table 2.1), although during the rising limb portions of the bed were covered with sand-sized sediment. As discharges decreased after the peak, the armor layer became more distinct.

FR 1

The primary sampling site in the upstream region of Fall River, FR 1, is located a few hundred meters upstream of the Highway 34 bridge within a 100-meter long straight stretch of

channel (Figure 2.2). The north bank consists of floodplain sediment (fine gravel and sand) deposited prior to the Lawn Lake flood. The south bank is stable and well-vegetated. The median grain size of the bed surface layer at this site is roughly 21 mm (Table 2.1), although portions of the bed were covered with sand-sized sediment supplied from Roaring River during much of the runoff season. As discharges reached lower levels after the peak, the armor layer became more distinct, lagging behind FR L by a couple weeks.

FR 2

The third site, FR 2, is located in the downstream area of Horseshoe Park, where the gradient of Fall River is lower and the sinuosity is higher (Figure 2.2). This site is located at the beginning of a straight stretch of river channel. Both banks are tall, steep, stable, and heavily vegetated by shrubs and grass. At this location, the bed surface grain size is about 8 mm (Table 2.1). This size more closely approximates the median grain size of the subsurface, and there is no distinct armor layer. Throughout the entire snowmelt season, the bed was characterized by continuous bed load transport and gently undulating sand dunes.

Cross Section Measurements

In addition to sampling sites, 49 unique cross sections were surveyed throughout the study area, resulting in one cross section roughly every 100 meters of channel length. Cross sections were chosen to avoid eddies, very unstable banks, log jams, and other debris which might affect the results of the measurements. Each cross section was measured at least twice throughout the season to provide enough information to investigate deposition or erosion.

Cross sections were monumented with wooden stakes placed several meters away from left and right banks. The spatial coordinates and elevations of each end point were recorded with

a mapping grade GPS (Trimble Geo 7x) and external antenna. Positions recorded in the field were subsequently post-processed to achieve a horizontal accuracy of < 15 cm for over 95% of the points.

Cross sections were surveyed using an engineering level and range pole. Elevations were recorded roughly every meter along the cross section, with the distance between measurements changing to capture important features like change in slope, top of bank, edge of water, and other physical features. Local and regional channel gradients were calculated with the use of bed elevation data provided by surveys and GPS measurements. Channel properties derived from cross sections measurements are listed in Table A1 of the appendix.

Bed Material Sampling

Bed surface grain size distributions were determined from pebble counts taken at roughly every other cross section of the study area. Samples were taken by laying a measuring tape along an exposed bar, representing bed conditions during higher flows, and measuring the size of about 100 grains with a hand-held gravelometer.

The subsurface sediment (bulk bed material) was sampled at the same locations as surface sediment for purposes of comparison. Subsurface samples were taken by removing the surface layer of sediment and taking a bulk sample of 1-5 kg of the sediment underneath. The size of the bulk samples varied to ensure that the largest grain in a sample did not exceed 5% of the total weight. Pebble count results for surface samples and grain size distributions for subsurface samples are detailed in Appendix A.

Discharge

Discharge was measured at all three sampling sites using the velocity-area method, with depth and velocity measurements recorded every 0.5 m along a cross section. Velocity measurements were taken using a Price AA current meter. The velocity measurements are converted to unit width discharges by multiplying by the local cross sectional area, and the total discharge for the cross section was found by summing these values. Discharge measurements were taken frequently (at least once a week) at every site to capture the complete range of flows characteristic of the runoff season.

Discharges measured at sampling sites were coupled with gage heights measured at the Highway 34 bridge to construct site-specific rating curves (Figure 2.4). When discharge was not measured the same day bed load was sampled, gage heights were recorded and converted to discharge using the relations from Figure (2.4). Discharge rating curves follow a power function of the form:

$$GH = aQ^b \qquad (2.1)$$

where Q is discharge, GH is gage height, and a and b define the shape of the power function.

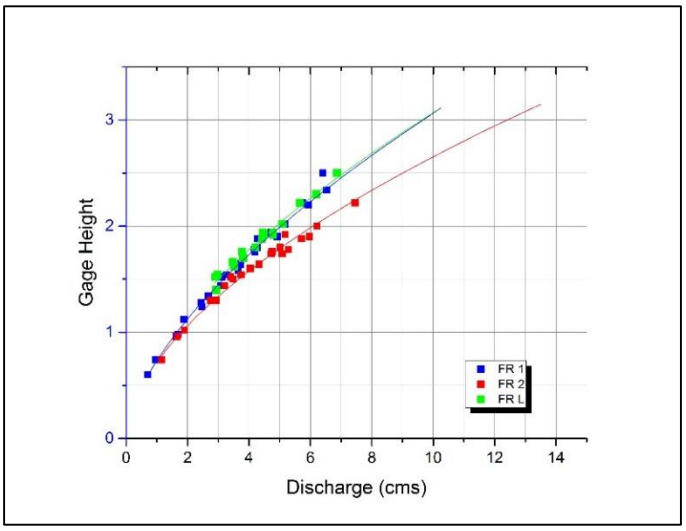

Figure 2.4. Discharge rating curves for FR L, FR 1, and FR 2. Relations between discharge and gage height follow power functions

Instantaneous Discharge Record

A synthetic, season-long hydrograph was created for Fall River using the 15-minute (instantaneous) records of discharge from a gage along the Big Thompson River in Moraine Park (USGS 402114105350101), about eight kilometers southwest of the study area. Discharge measurements taken at the three sampling sites, (FR L, FR 1, and FR 2), were matched in time to the appropriate measurement at the USGS gage to develop scaling relations for each sampling site (Figure 2.5). Discharges at FR L and FR 1 have nearly identical scaling values, 0.5959 and 0.5961, respectively; discharge increases at FR 2, however, to a value of 0.7561.

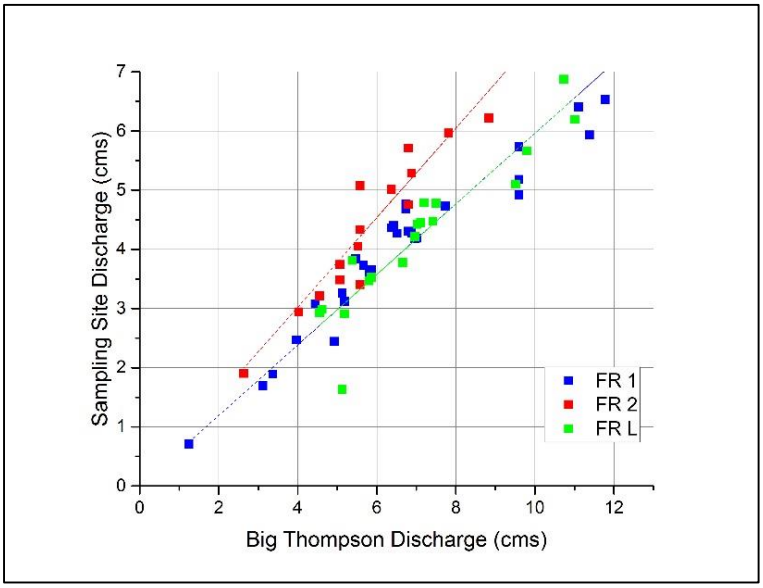

Figure 2.5. Discharge scaling relation for sampling sites showing relation between Fall River and Big Thompson River discharges.

The resulting hydrographs (Figure 2.6) show a steep rising limb to an early peak discharge at the end of May, around Memorial Day. The falling limb is much more gradual, accented by minor peaks during periods of significant precipitation, in mid-June and early August.

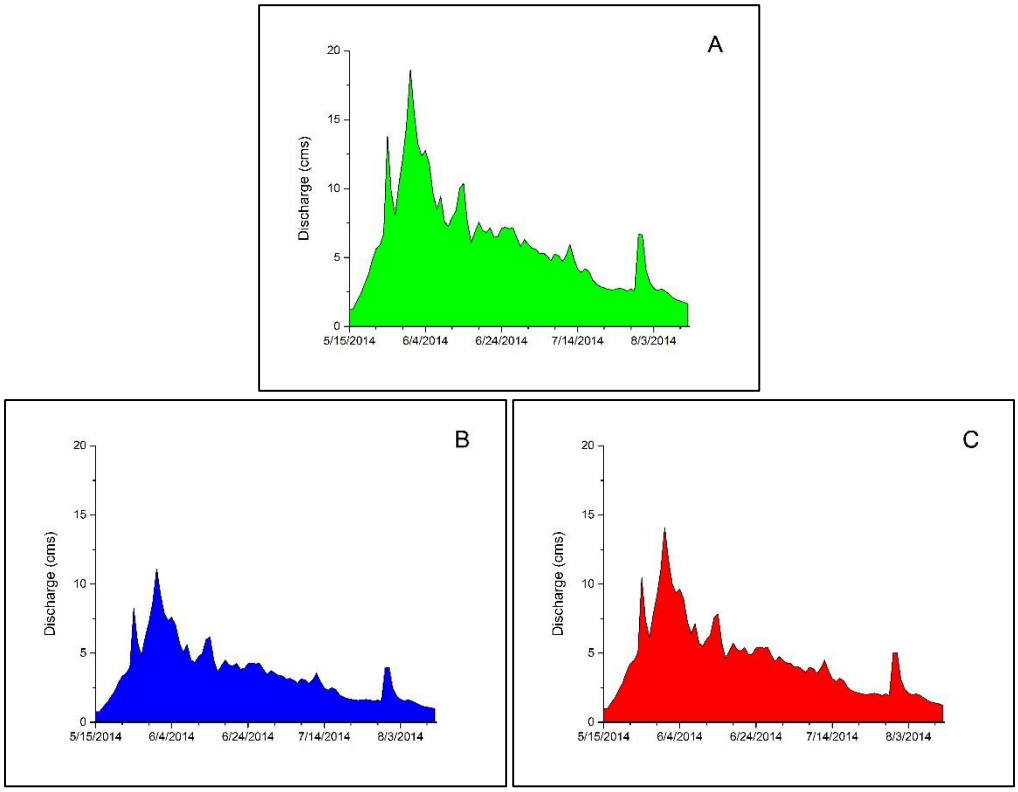

Figure 2.6. a) Big Thompson Hydrograph, and Synthetic Fall River Hydrograph at b) FR 1 and c) FR 2

Sediment Transport Measurements

Bed load measurements were taken at FR L, FR 1, and FR 2 using an Elwha River sampler with a 10 × 20 cm orifice [*Clayton and Pitlick*, 2007]. Bed load was sampled at various lateral positions, or verticals, spaced one meter apart along each cross section; mass collection times at each vertical varied between 30 seconds and two minutes depending on the flow rate. During each measurement, the sampler was positioned flat on the bed, orthogonal to the flow of water, and care was taken not to disturb the surrounding sediment. A total of 58 separate bed load samples were taken, 13 samples at FR 1, 25 at FR 1, and 20 at FR 2 over a three month period from May 15 to August 12. For each bed load sample, individual loads from each vertical were combined to create a transport rate representative of the entire cross section. Unit bed load

transport rate, q_b (kg/m/s), was calculated by dividing the total weight sampled by the sampled width and sampling time per vertical.

Figure 2.7. Typical bedload sampling procedure with Elwha sampler, shown at FR 1 (left), and close-up of Elwha sampler (right)

Samples of the bed load and subsurface bed material were sieved in the lab to determine grain size distributions. Samples were oven-dried for at least 24 hours and organic material not representing transport was removed prior to weighing each sample for use in grain size distributions and transport rate calculations. Each sample was sieved at 1/2 ψ intervals to determine the grain size distribution, where

$$\psi = \frac{\log D}{\log 2} \qquad (2.2)$$

and D is in millimeters. A numerical interpolation program was used to calculate the important percentiles D_{84}, D_{50}, D_{64}, from the grain size distributions, where the subscripts represent the percentage of particles finer than a given grain size. All grain size distributions from bed load are detailed in Appendix A.

While not directly monitored, Roaring River's influence on the Fall River is unmistakable. Three days were spent hiking along Roaring River from Lawn Lake to the confluence with Fall River to observe areas of destabilized sediment in its channel. These destabilized segments were pervasive throughout the river, especially in steep segments of the river, and were well documented photographically.

Channel Characteristics

Bankfull downstream hydraulic geometry relations were developed for the study area based on the data collected at each cross section from topographical surveys. Bankfull cross sectional area was found by summing trapezoidal areas computed from depth-width measurements along a cross section. Cross-sectional width was defined as the distance between the top of bank measurements during surveys. Average cross-sectional depth was then calculated by dividing the area by the width.

Downstream trends in bed elevation, slope, and median surface grain size were found by fitting the data with the three-parameter exponential function,

$$P = C_0 + C_2 e^{-\alpha x} \qquad (2.3)$$

where P is the parameter in question, C_0 is an asymptotic value for the exponential trend, C_2 is a constant of proportion, α reflects the rate at which the exponential trend declines, and x is the distance downstream. Depth, however, was fit to a linear trend.

The best-fit relations for mean depth, slope, and grain size were then used to evaluate trends in shear stress, τ, and dimensionless shear stress, τ*. For steady, uniform flow, the average boundary shear stress is defined by the slope-depth product as:

$$\tau = \rho g R S \qquad (2.4)$$

where ρ is the density of water, g is the gravitational acceleration, R is the hydraulic radius, and S is the slope. Where rivers are sufficiently wide, the hydraulic radius may be approximated as the water depth, H, as was the case in this study. A three-parameter exponential function was also fit to shear stress values calculated at each cross section.

Flow and Sediment Transport Relations

Sediment transport rates were calculated from two sets of empirical relations: discharge-based transport relations and Parker's shear stress-based transport relations. The first approach relates the measured volumetric water discharge, Q (m^3/s), to the measured sediment transport rates, Q_s (kg/s), by a power function:

$$Q_s = aQ^b \qquad (2.5)$$

where a and b are adjustable parameters used to fit the function to the measurements.

For the shear stress-based approach, we use two transport functions developed by *Parker* [1979; 1990]. These functions can be written together as:

$$W^* = \begin{cases} 11.2\left(1 - \frac{0.853}{\phi}\right)^{4.5} & \phi \geq 0.853 \\ 0.002\phi^{14.2} & \phi < 0.853 \end{cases} \qquad (2.6)$$

where W^* is a dimensionless transport rate and $\phi = \tau^*/\tau_r^*$ is the transport stage. W^* is defined as:

$$W^* = \frac{(s-1)gq_b}{\rho_s\left(\frac{\tau}{\rho}\right)^{1.5}} \qquad (2.7)$$

where s is the specific gravity of sediment (2.65), g is gravitational acceleration, q_b is the unit-width sediment transport rate (kg/m/s), ρ_s is the density of sediment (2650 kg/m^3), τ is the average boundary shear stress (N/m^2), and ρ is the density of water (1000 kg/m^3). Transport stage, ϕ, is a ratio of dimensionless shear stresses, called Shields stresses. The subscript r in the

transport stage definition refers to a reference value of τ^*, which produces small, but non-negligible transport rates. Shields stress is defined as:

$$\tau^* = \frac{\tau}{(s-1)\rho g D_{50}} \qquad (2.8)$$

where D_{50} is the median grain size of the bed.

The shear stress corresponding to each bed load sample was calculated by:

$$\tau = \rho g S^{1/4}(nU)^{3/2} \qquad (2.9)$$ or,

$$\tau = \frac{(Un)^2 \rho g}{H^{1/3}} \qquad (2.10)$$

where n is Manning's roughness coefficient, U is velocity, and H is the depth. Both equations combine common variables of the average boundary shear stress equation (2.4) and Manning's flow resistance equation:

$$U = \frac{H^{2/3} S^{1/2}}{n} \qquad (2.11)$$

where the common variables in equations (2.9) and (2.10) are depth and slope, respectively.

Parker's transport functions are calibrated to Fall River by adjusting the value of τ_r^* to fit our sampling data. According to *Parker* [1982], an acceptable value of τ_r^* occurs when W^* equals 0.002. We can then find the τ_r^* graphically by plotting data from transport measurements in the form of curves of τ^* versus W^*. Once calibrated, W^* values can be converted to dimensional unit-width transport rates, q_b (kg/m/s), by:

$$q_b = \frac{W^* \rho_s \left(\frac{\tau}{\rho}\right)^{1.5}}{(s-1)g} \qquad (2.12)$$

For each empirical transport relation, sediment transport rates are calculated from the time series of discharges available for 2014, yielding a time series of sediment transport rate. Integrating the area under these curves yields the annual sediment load estimates for 2014.

Chapter III: Results

Downstream Trends in Channel Geometry, Slope and Grain Size

Downstream trends in the average bankfull depth and bankfull width of Fall River showed a slight increase and decrease, respectively, across the 52 sites of the study area (Figure 3.1). Across the study area, the average bankfull depth varies over a relatively small range, from 0.4 to 1.3 m, with more than 60% of the data between 0.6 and 1 m. Bankfull width varies by a larger range throughout the study area, from about 8 to 21 m, excluding one outlier.

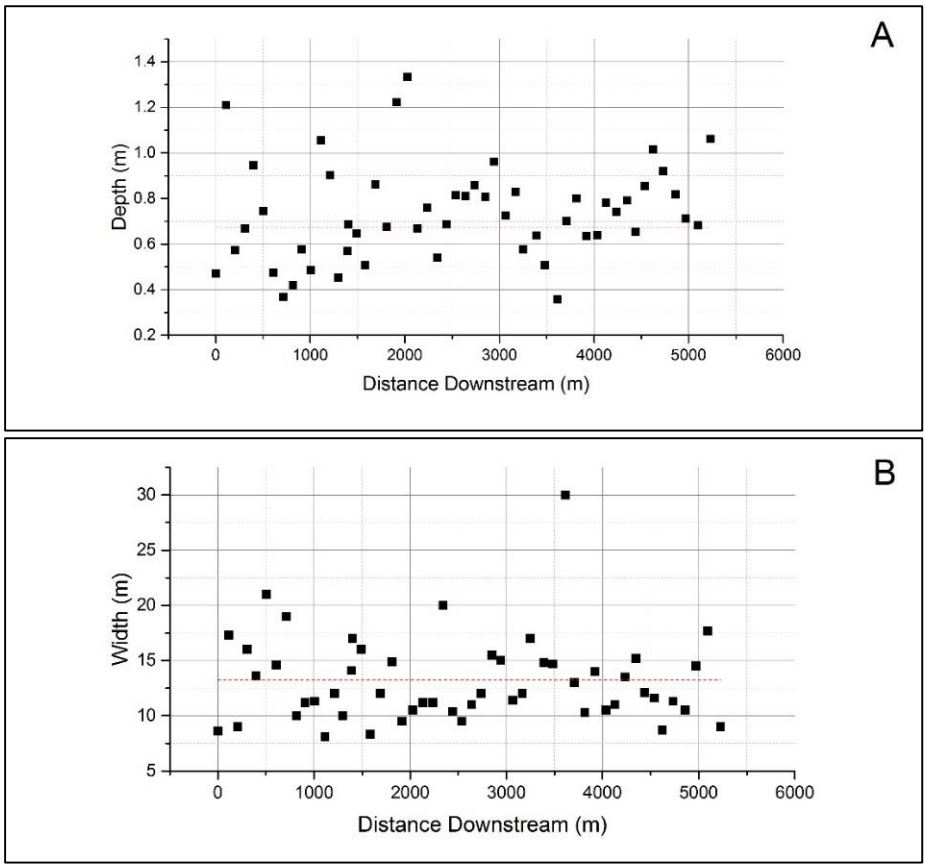

Figure 3.1. Downstream trends in a) mean depth and b) width (one outlier removed). Data fitted with linear trends.

A wide scatter in width occurs in the upstream portions of Fall River, where the effects of bank erosion during the 2013 flood impacted the geometry of the channel. In contrast, there is less scatter in width in downstream portions of Fall River, where the banks are heavily vegetated

and thus much more resistant to erosion. As a result, width remains relatively constant downstream, with a mean value of about 13.1 m. Goodness-of-fit tests of the downstream relations for bankfull depth and width indicate that neither trend is statistically significant ($p > 0.1$), even with the one outlier removed for width (Table 3.1).

Table 3.1. Parameter Values and Summary Statistics for Regression Relations Shown in Figure 3.1, One Outlier Removed for Width Analysis

	Slope	Intercept	R^2	t-statistic	*p*
Depth	2.71e-5	0.67	0.04	1.41	0.16
Width	-1.98e-4	13.3	0.009	0.68	0.50

The longitudinal profile of Fall River is concave up, with the mean bed elevation and slope decreasing exponentially across the study area (Figure 3.2).

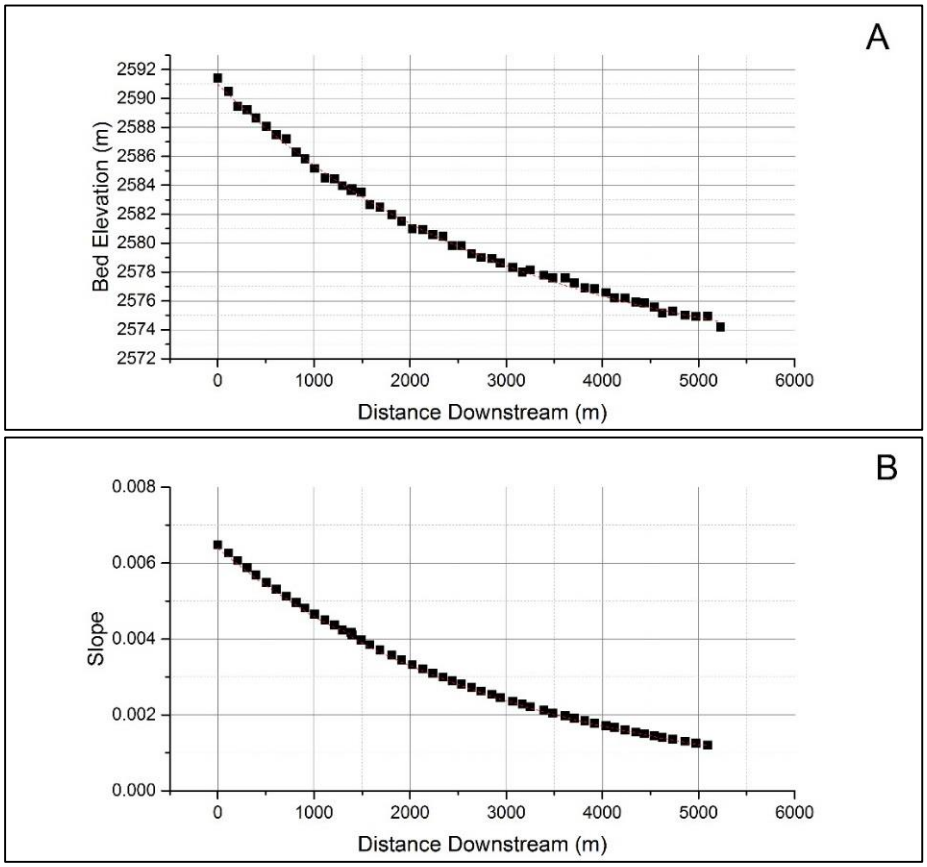

Figure 3.2. Downstream trends in a) mean bed elevation, and b) bed slope. Data were fit with three-parameter exponential functions.

The exponential shape reflects the change between upstream (straighter, higher gradient) and downstream (sinuous, lower gradient) regions of the study area. When plotted at this scale, the trends in mean bed elevation and slope (which are based on mean bed elevation) appear to be relatively smooth.

The trend for slope was calculated across three cross sections, to remove some of the local variability. The trends for bed elevation and slope were fit with a three-parameter exponential function, which takes the general form

$$y = C_0 + C_2 e^{-\alpha x} \quad (3.1)$$

where C_o is an asymptotic value for the exponential trend, C_2 is a constant of proportion, α is a shape parameter, and x is distance downstream. Goodness-of-fit tests of the relations for bed elevation and slope indicate that both trends are statistically significant ($p << 0.001$) (Table 3.2).

Table 3.2: Parameter Values and Summary Statistics for Regression Relations Shown in Figure 3.2

	C0	C2	α	R^2	t-statistic	*p*
Bed Elevation	2571	20	-0.00033	0.998	156.45	« 0.001
Slope	0	0.0066	-0.0003	0.999	184.60	« 0.001

Downstream trends in the median grain size, D_{50}, of the surface and subsurface sediment also showed exponential decreases across the study area (Figure 3.3). Surface D_{50} ranged from about 50 mm in the vicinity of the alluvial fan to < 10 mm at the point where Fall River exits Horseshoe Park. The wide range in D_{50} in the upstream portion of Fall River is due to variable amounts of deposition associated with the 2013 flood. The downstream fining trend may also be interpreted as a result of selective transport of finer grains, resulting in the longitudinal sorting of grain sizes. Subsurface D_{50} decreased across the study area from about 20 mm to 2 mm. The same general trend observed in the surface grain size existed in the subsurface, though the largest grain sizes in the upstream section were not present in the subsurface samples.

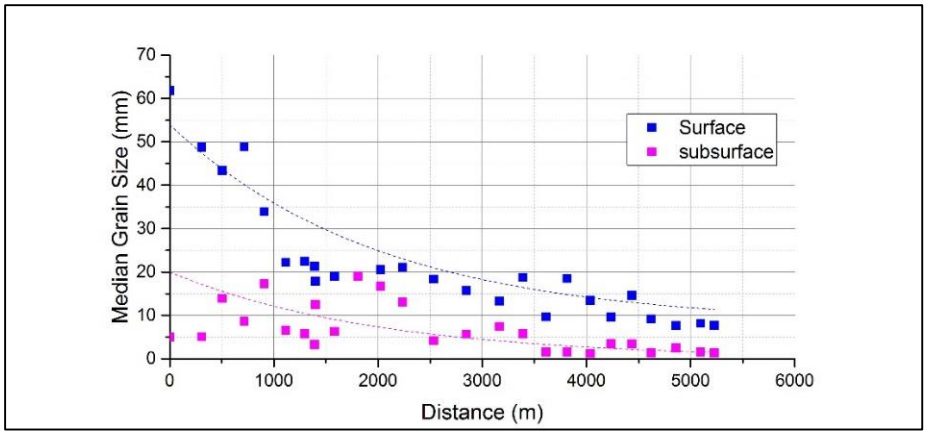

Figure 3.3. Downstream trend in median grain size, D50, (mm) of surface and subsurface. Data were fit with three-parameter exponential functions.

These trends indicate that less surface coarsening occurred downstream where the sediment supply was generally higher. Goodness-of-fit tests of the grain size relations indicate that both trends are statistically significant ($p < 0.005$) (Table 3.3).

Table 3.3: Parameter Values and Summary Statistics for Regression Relations Shown in Figure 3.3

	C0	C2	α	R^2	t-statistic	*p*
Surface	8	46	-0.0005	0.721	7.87	« 0.001
Subsurface	0	20	-0.0005	0.393	3.77	0.001

Shear Stress

The downstream trend in bankfull shear stress showed an exponential decrease across the study area (Figure 3.4a, next page). These values were calculated with eqn. 2.4, using the local bankfull depth and the reach average slope given by the relation shown in Figure 3.2b. While bankfull shear stress varied locally due to differences in depth, the overall trend was controlled primarily by the decrease in slope. The effect of slope on bankfull shear stress is represented quantitatively in the identical values of the parameter α in the slope and bankfull shear stress trend functions. Consequently, the bankfull shear stress decreases by roughly a factor of four,

from values of about 40 N/m^2 in reaches downstream of the alluvial fan to values of about 10 N/m^2 in lower Horseshoe Park.

The downstream trend in bankfull Shields stress, τ^*, shows essentially no change across the study area (Figure 3.4b). To factor in the effect of surface grain size on shear stress, bankfull Shields stress values were calculated using eqn. 2.7, with the local bankfull depth and slope, and the surface grain size estimated from the trend shown in Figure 3.3. Values of τ^* scatter over nearly an order of magnitude, from 0.028 to 0.111, but nearly 80% of the data fall between 0.04 and 0.08. The nearly constant trend in Shields stress is a result of the trends in slope and grain size decreasing at nearly the same rate, with exponents of -0.0003 and -0.0005, respectively.

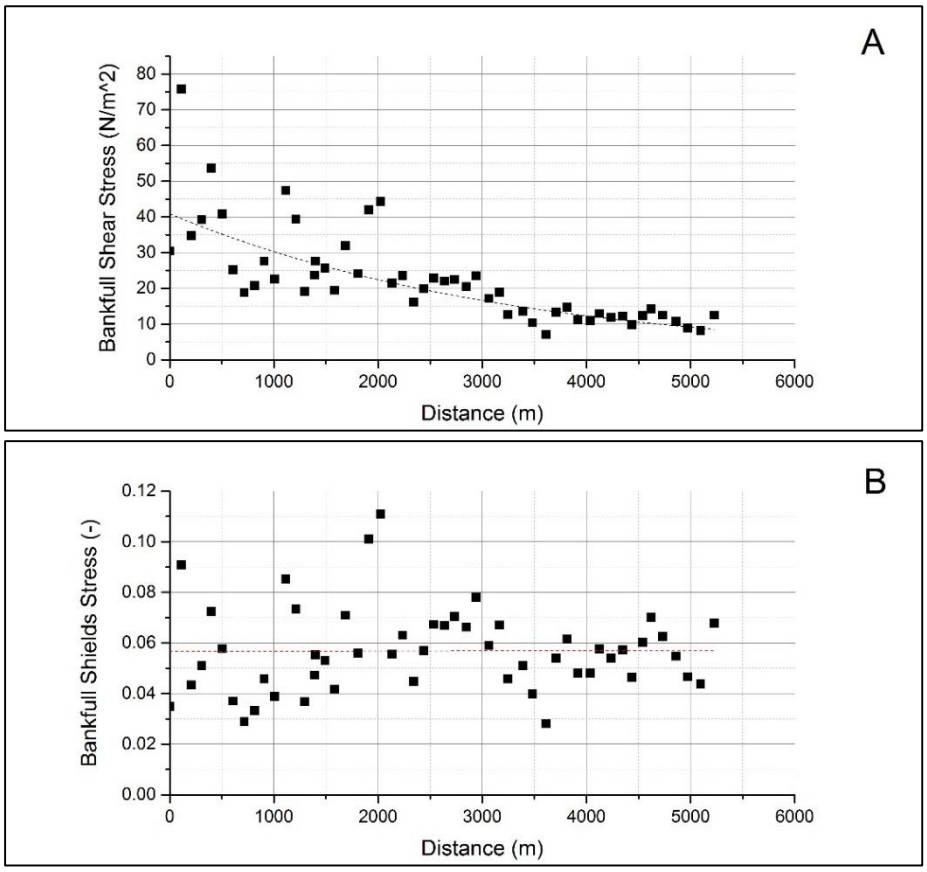

Figure 3.4. Downstream trends in bankfull a) shear stress (fit with exponential trend), and b) Shields stress (fit with linear trend). Estimates of shear stress were calculated using eqn. 2.3 with the water depth at bankfull conditions and the appropriate slope given by the trend from Figure 3.2b. Estimates of Shields stress were calculated using eqn. 2.4 with shear stress values from Figure 3.4a and surface grain size given by the trend in Figure 3.3.

The goodness-of-fit test of the shear stress relation indicates that the trend is statistically significant ($p << 0.001$), but the trend in Shields stress is not statistically significant, even with two outliers removed (Table 3.4).

Table 3.4. Parameter Values and Summary Statistics for Regression Relations for Shear Stress and Shields Stress (two outliers removed) Shown in Figure 3.4

	C0	C2	α	R^2	t-statistic	*p*
Shear Stress	0	40.863	-0.0003	0.748	7.96	« 0.001
	Slope		Intercept	R^2	t-statistic	*p*
Shields stress	6e-7		0.0548	0.065	0.45	0.65

Annual Sediment Loads Calculations

To quantify the mass of sediment transported through the study area in 2014, empirical relations between discharge and bed load transport were created at the two sampling sites where measurements were most complete, FR 1 and FR 2. These empirical relations were used in conjunction with the time series of instantaneous (15-minute) discharges shown in Figure 2.6 to calculate transport rates for every 15-minute interval throughout the 2014 season. Integrating each value over its time interval and summing these instantaneous loads gave the annual sediment load for each site.

We examined the effects of using two different approaches to formulate empirical transport relations at FR 1 and FR 2. In the first approach, we created an empirical relation between water discharge and bed load transport rates using the measured data collected throughout 2014. In the second approach, we calibrated the reference shear stress value in the bed load transport function of *Parker* [1979] described in Chapter 2, then modeled bed load transport rates as a function of shear stress, estimated for each 15-minute interval of discharge. While constantly measuring sediment transport directly would provide very accurate results, doing so is impractical and the field work is time-consuming. Instead, measured data can be used

to calibrate transport relations, which allows us to estimate sediment transport based on data we can measure continuously, like discharge. Parker's function has more physical basis than discharge-based empirical relations, since it relates sediment transport to physical parameters not captured by discharge – grain size and slope. These two parameters have a significant impact on sediment transport. Thus, both of these relations were used to calculate annual sediment loads to evaluate the difference in the estimates found by each approach.

Sediment Rating Curves

The first approach to calculate annual sediment loads used discharge as the independent variable to predict sediment transport. Sediment rating curves, relating discharge to transport rates by a power function, were created for FR 1 and FR 2 (Figure 3.5). For FR 1, the sediment rating curve is separated into two relations, one representing measurements taken prior to the peak discharge, the other representing measurements taken after the peak. For FR 2, two data points collected on July 8th and July 17th were removed as outliers.

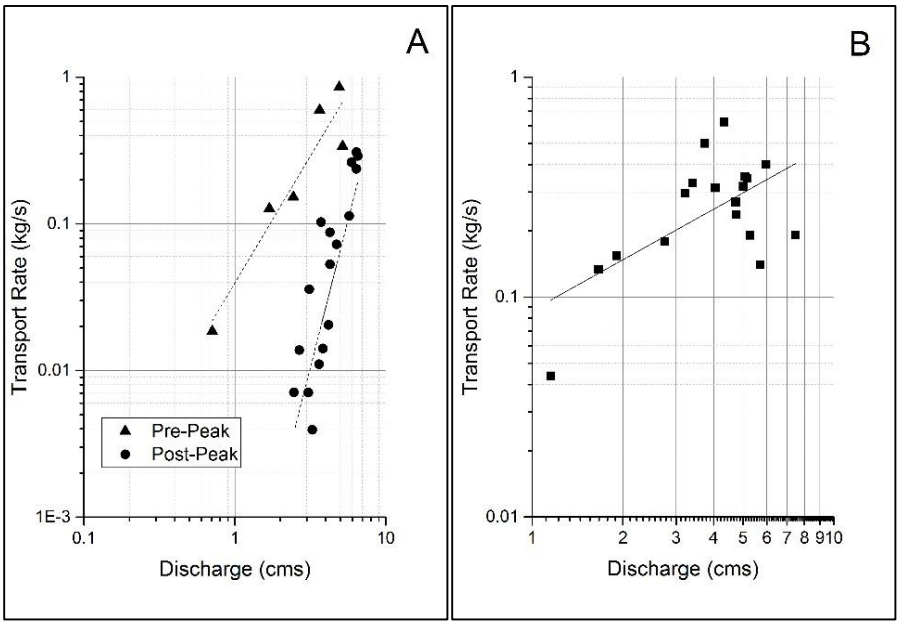

Figure 3.5. Sediment rating curves, relating transport rates to discharge by a power function for a) FR 1 (two relations are shown representing the two sites, 20 meters apart) and b) FR 2 (two data points from July 8th and July 17th were removed as outliers).

The empirical relations for FR 1 were much steeper than the relation for FR 2. The goodness-of-fit of the sediment rating curves for FR 1 and FR 2 are both statistically significant, with FR 1's data resulting in a stronger relation ($p < 0.005$) than FR 2 ($p < 0.05$) (Table 3.5). Using the transport relations presented above and the time series of daily discharges, we estimate that the total loads at FR 1 and FR 2 for 2014 were 1,570 Mg and 3,640 Mg, respectively.

Table 3.5. Parameter Values and Summary Statistics for Discharge-Based Sediment Rating Curves at FR 1 and FR 2 (Two Data Points Removed as Outliers)

	a	b	R^2	t-statistic	*p*
FR 1, May 15-May 28	0.0396	1.7273	0.90	6.028	0.004
FR 1, May 29-Oct 14	0.0017	2.3682	0.61	5.154	0.00008
FR 2	0.087	0.7637	0.25	2.362	0.03

Reference Shear Stress Analysis

The second approach used to calculate annual sediment loads involved fitting the bed load transport relations of *Parker* [1979; 1990] to the field measurements, then using the fitted relations to estimate daily loads as a function of shear stress. For each bed load measurement, we used eqn. 2.12 to convert the mass transport rate per unit width to a dimensionless transport rate, W*, then plotted those values against the dimensionless shear stress, τ^*, estimated from eqns. 2.8 and 2.9. The results are presented in Figure 3.6, along with the transport functions of *Parker* [1979; 1990]. Recall that Parker's transport function requires an estimate of the reference shear stress, τ_r. For each site, the reference shear stress was adjusted in the transport function until the function was calibrated to the measured data. These three values of τ_r were then converted to reference Shields stress, τ_r^*. The values of reference shear stress and reference Shields stress for each sampling site are shown in Table 3.6.

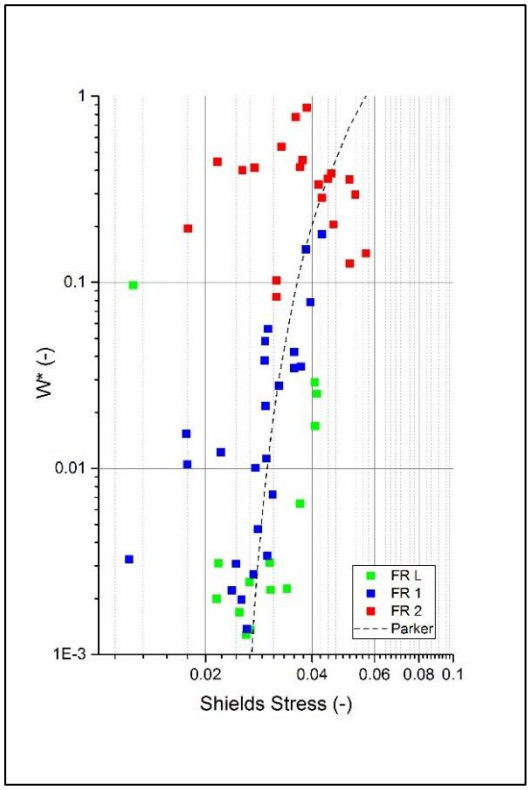

Figure 3.6. Plot of W versus τ for sampling sites FR L, FR 1, and FR 2, used to find reference Shields stress for each site. The dashed line represents the transport function of Parker [1979], calibrated to each site's reference shear stress. One dashed line is shown because all three sites possess the same reference Shields stress.*

	Table 3.6. Reference Shear Stress and Shields Stress for All Three Sampling Sites		
	τ_r (N/m^2)	$D_{50,surf}$ (mm)	τ_r* (-)
FR L	20.0	44	.028
FR 1	14.2	31	.028
FR 2	5.2	11	.028

Because of the similarities between FR L and FR 1, these two sampling sites tend to collapse to a common trend line, suggesting that the sediment at each site is entrained at the same reference Shields stress, $\tau_r^* = 0.028$. Despite the scatter in the data set for FR 2, a combination of changes in slope, depth, and bed textures resulted in the same reference Shields stress as the other two sampling sites, $\tau_r^* = 0.028$. These reference Shields stresses equate to reference flow rates of 3.6, 3.6, and 2.4 cms for FR L, FR 1, and FR 2, respectively.

When plotted as unit-width transport rates, Parker's transport function shows good agreement with the measured values (Figure 3.7). Pairs of measured and estimated transport rates were also plotted together to analyze the fit of the calibrated transport functions (Figure 3.8). The analysis of data shows relatively good agreement between the measured and estimated transport rates overall. The coefficient and exponent of the trend for data with perfect agreement would be 1; the coefficient and exponent of the trend line in Figure (3.8) are 1.17 and 1.07. For the range of transport rates measured, the trend line (dashed line) indicates that estimated values are typically slightly lower than measured values, with the differences between estimates and measured values increasing as transport rates decrease.

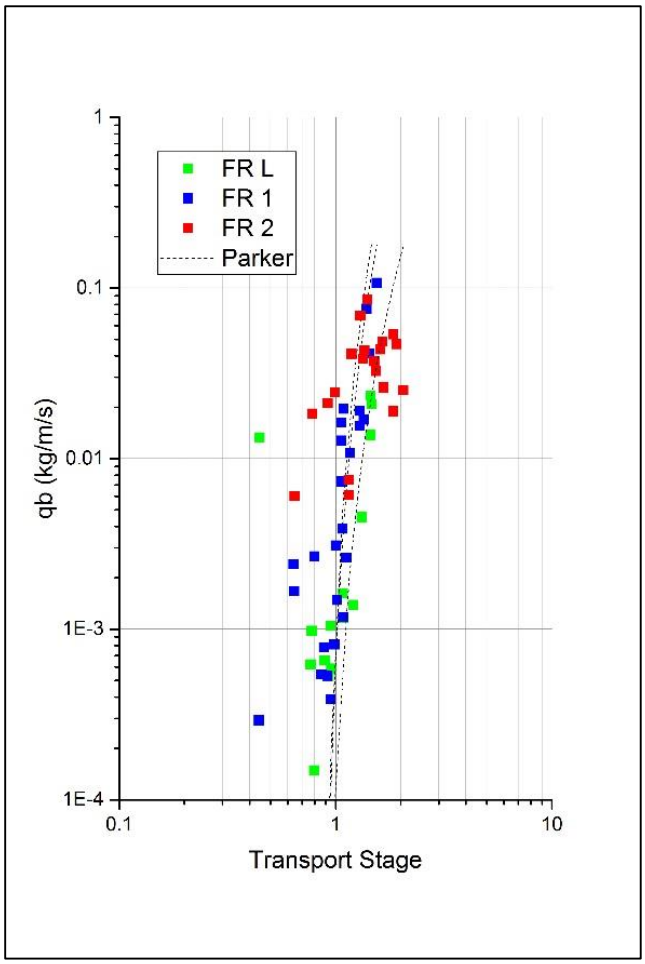

Figure 3.7. Unit-width transport rate versus transport stage, q_b v ϕ, at FR L, FR 1, and FR 2. Lines represent calibrated transport relations.

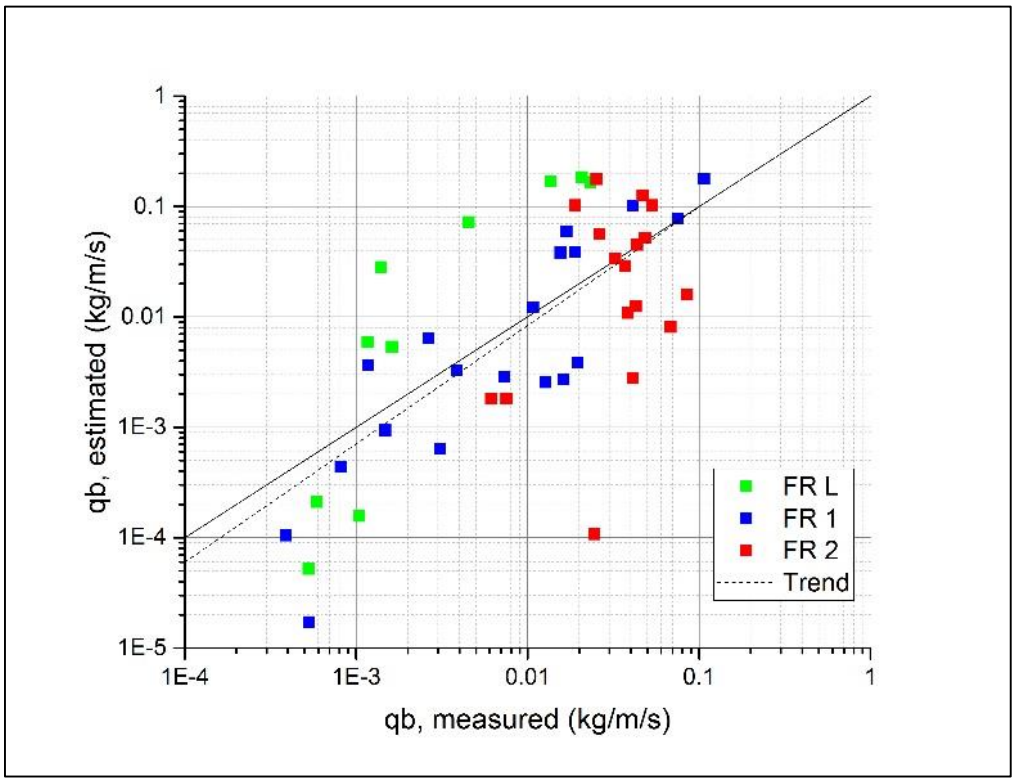

Figure 3.8. Comparison between measured and predicted bed load transport rates. Solid line represents 1:1 relationship; dashed line represents a power law fit to data from all three sites. All data with transport stage less than 0.9 removed.

Time Series Trends in Bed Load Transport and Grain Size

Measurements of bed load taken over the course of the field season show that transport rates at FR1 mimicked the rise and fall of the hydrograph (Figure 3.9), whereas at FR2, transport rates remained high into late summer, even as discharge dropped. A similar pattern is evident in the trends in grain size (Figure 3.10), where the texture of the bed load at FR1 first increased then decreased, but at FR2 remained roughly the same throughout the summer.

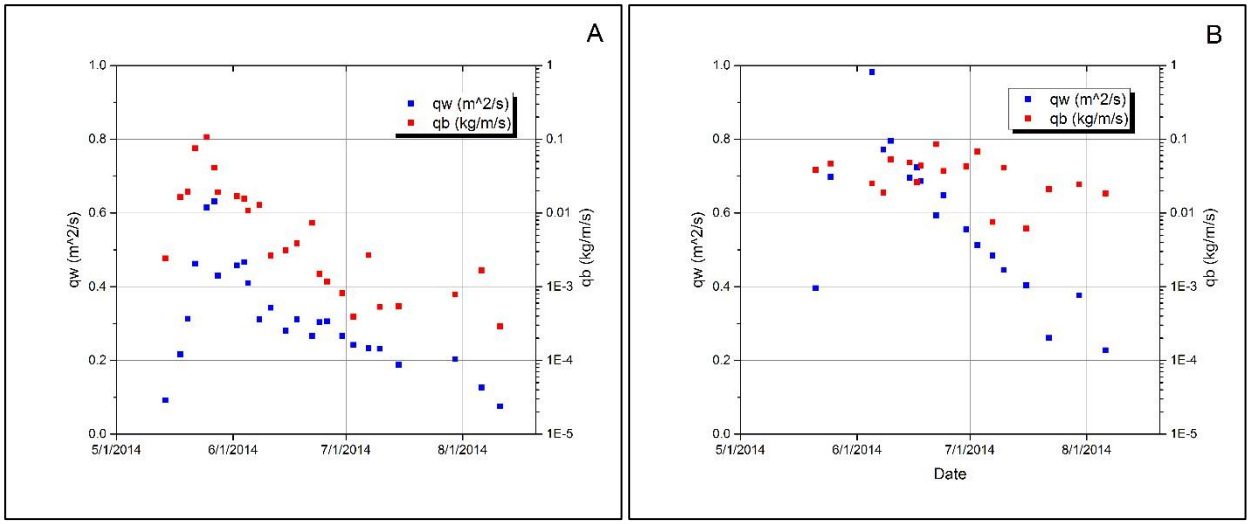

Figure 3.9. Measured unit-width discharge, q_w, and unit-width bed load transport, q_b, versus time for a) FR 1, and b) FR 2. Blue data points are q_w; red data points are q_b.

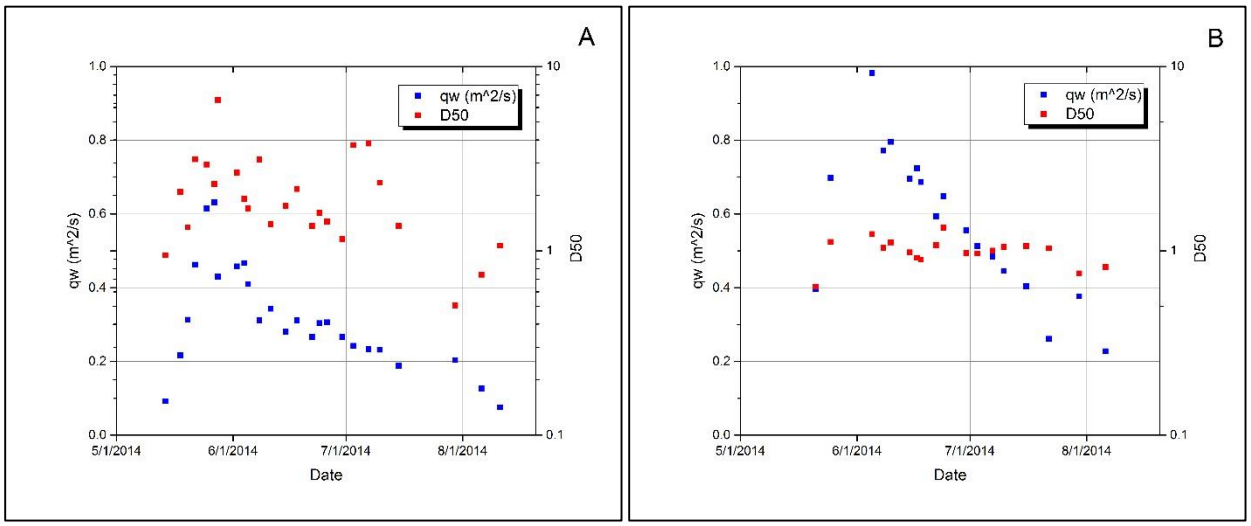

Figure 3.10. Measured unit-width discharge, q_w, and median grain size in mm, D_{50}, versus time for a) FR 1, and b) FR 2. Blue data points are q_w; red data points are D_{50}.

Annual Sediment Loads

Annual sediment loads calculated using eqn. 2.10 were 3,022 Mg and 4,648 Mg at FR 1 and FR 2, respectively; annual sediment loads calculated using eqn. 2.11 were 1,607 Mg and 4,436 Mg at FR 1 and FR 2, respectively (Table 3.7). The following table summarizes the annual sediment loads calculated for FR 1 and FR 2 from the discharge-based approach and the two

shear stress-based approaches. The shear-stress based approaches tend to estimate higher annual sediment loads than the discharge-based approach.

Table 3.7. Annual Loads Calculated from Discharge-Based and Shear Stress-Based Empirical Sediment Transport Relations		
	FR 1 (Mg)	FR 2 (Mg)
Q-based Relation	1,570	3,640
τ-based Relation, equation 2.10	3,008	4,648
τ-based Relation, equation 2.11	1,343	4,436

Cross Sectional Surveys and Geomorphic Sediment Budget

Repeat surveys at each cross section provide temporal information about the width, depth, and slope of the channel, as well as a means to calculate a geomorphic sediment budget by quantifying erosion and deposition throughout the study area. Changes in mean bed elevation due to erosion or deposition were calculated by taking the difference between the two surveys (Figure 3.11). The mass of erosion or deposition was found by multiplying the change in cross sectional area by the distance halfway to each adjacent cross section, then multiplying by a bulk density of bed sediment, 1500 kg/m^3, given by *Pitlick* [1993].

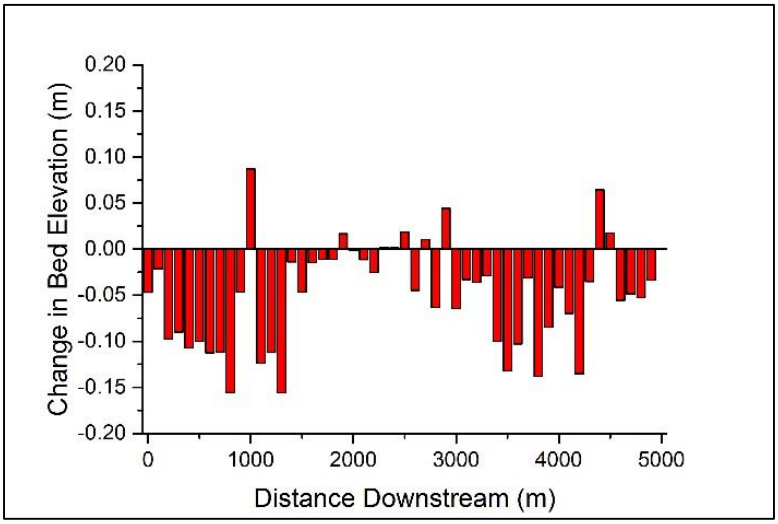

Figure 3.11. Change in bed elevation across the study area. Positive values indicate an increase in bed elevation; negative values indicate a decrease in bed elevation.

The time frame over which the two cross sectional surveys at a given site occurred varied from location to location. For the entire study area, the first round of surveys occurred between May 15 and June 26; the final round of surveys occurred between June 10 and October 23. The results of the geomorphic sediment budget can be compared to annual sediment loads calculated by the empirical bed load transport relations. The annual sediment load estimated for FR 1 should be similar to the net erosion of sediment between XS 0 and FR 1. The annual sediment load estimated for FR 2 should be similar to the net erosion of sediment between FR 1 and FR 2, plus the amount of sediment transported past FR 1. Based on cross section surveys, the annual load estimated at FR 1 is 2,303 Mg, which is about 700 Mg smaller than the load estimated by the shear stress-based relation using eqn. 2.10, 3,008 Mg. Using this annual sediment load for FR 1 and the amount eroded between FR 1 and FR 2 from the geomorphic budget, the annual load estimated at FR 2 is 5,483 Mg, which is about 850 Mg larger than the load estimated by the shear stress-based relation using eqn. 2.10, 4,648 Mg.

Change in bed elevation across the study area never surpassed a gain or loss of 0.16 m. A majority of the cross sections increased in depth, resulting in erosion of bed sediment. Moreover, this change in bed elevation is likely from expulsion of sediment stored in the channel during the flood. A statistical analysis of the temporal change in bed elevation indicates that this physical parameter did not vary significantly throughout 2014, (t statistic = 35; $p \ll 0.001$). While the changes in bed elevation are statistically small, the results of the geomorphic sediment budget indicate that a substantial amount of sediment was eroded throughout Fall River's channel.

Chapter IV: Discussion and Conclusions

The results of our field study indicate that in the first year following the 2013 flood, Fall River was able to transport a majority of sediment supplied by Roaring River, along with sediment eroded from within its channel, with only small changes in bed elevation and adjustments of surface grain size. While annual sediment loads increase from FR 1 to FR 2, a geomorphic sediment budget estimated from changes in cross sectional area compares favorably to the annual sediment loads estimated from sampling at each site.

The geomorphic characteristics of Fall River vary downstream systemically, generating sufficient shear stresses to maintain sediment transport throughout the study area, with a nearly constant bankfull Shields stress, ~0.056. Analysis of bed load and discharge data indicates that bed load begins moving at the same reference Shields stress, 0.028, at all three sampling sites spanning the study area. As a result, Fall River has bankfull dimensions which generate a Shields stresses roughly twice the threshold for motion, in response to systematic changes in slope and grain size along its channel. Therefore, the morphology of Fall River's channel is maintained by flows in excess of the threshold for sediment motion.

Investigations of downstream trends in channel properties of other gravel bed rivers provide a comparison to Fall River. On the Allt Dubhaig in Scotland, *Ferguson and Ashworth* [1991] observed a decrease in surface grain size due to a decline in slope from 0.02 to 0.00015. Unlike Fall River however, the downstream decrease in slope of the Allt Dubhaig is much greater than for surface grain size and constant bankfull Shields stress is not maintained, resulting in a decrease in bed load transport capacity downstream. Additionally, changes in width were limited by stable bank vegetation, a condition consistent with Fall River. On the Colorado River, *Pitlick and Cress* [2002] observed a large increase in depth, relative to width, in response

to a five-fold decrease in slope and a two-fold decrease in grain size. Here, the combination of changing channel characteristics results in a constant bankfull Shields stress along the Colorado River. This result is consistent with Fall River, except that Fall River primarily adjusts surface grain size to maintain transport.

Using the calibrated sediment transport relations, we estimate annual sediment loads of 3,008 Mg and 4,648 Mg in 2014 for FR 1 and FR 2, respectively. The difference in loads does reflects differences in the processes occurring across the study area. In chapter 3, the determination of the reference Shields stress, 0.028, equates to reference flow rates of 3.6 cms and 2.4 cms for FR 1 and FR 2, respectively. Based on the time series of instantaneous discharges at each site, the reference discharge was exceeded for 38 days at FR 1 and 65 days at FR 2. Therefore, the flow at FR 2 was sufficient to transport sediment supplied to it more frequently resulting in a greater annual sediment load than at FR 1.

As a check of the transport relations, loads estimated from changes in channel cross sections compare favorably to the loads estimated from transport relations. To estimate sediment loads from the geomorphic sediment budget, the mass of erosion across the study area was tracked by changes in cross sectional area between surveys (Figure 4.1).

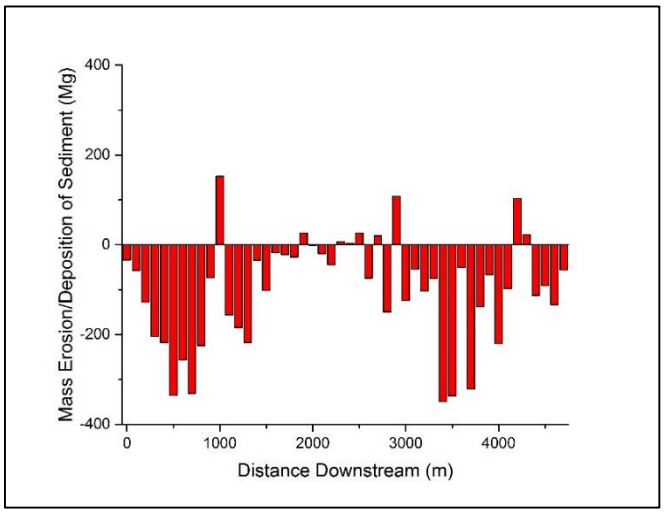

Figure 4.1. Mass of erosion (-) and deposition (+) across study area in 2014. Approximate XS distances used.

Total cumulative erosion calculated from the geomorphic sediment budget was 2,303 Mg from XS 0 to FR 1 and 2,475 Mg from FR 1 to FR 2. The sediment load between XS 0 and FR 1 from the geomorphic sediment budget equates to ~75% of total bed load transported at FR 1, where the additional 25% of sediment transported at FR 1 was supplied directly from Roaring River during 2014. The sediment eroded between FR 1 and FR 2, plus the sediment transported past FR 1, results in an estimated annual load of 5,483 Mg at FR 2. This estimated load is ~18% greater than the 4,648 Mg estimated from the sediment rating curve.

The volume of sediment carried by Fall River in 2014 is high in comparison to other gravel bed rivers where these estimates have been made. *Mueller and Pitlick* [2013] estimated annual sediment yields (m^3/yr) for a range of rivers and streams in snowmelt-dominated basins and related these values to their bankfull bed load transport rate (m^3/s). The equivalent data for FR 1 and FR 2 in 2014 were plotted alongside this data set, showing that Fall River follows the same trend (Figure 4.2).

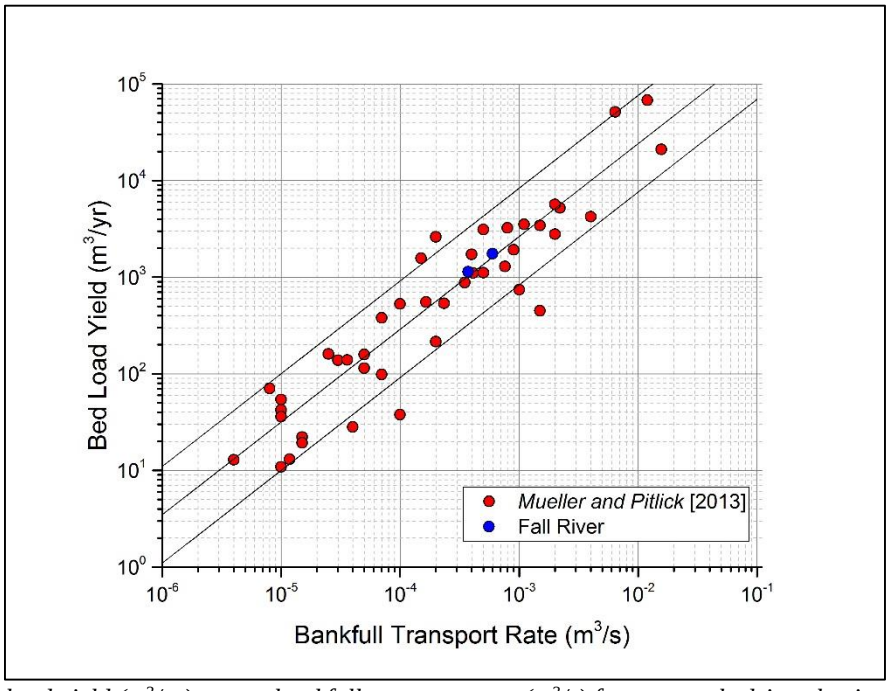

Figure 4.2 Bed load yield (m^3/yr) versus bankfull transport rate (m^3/s) for snowmelt-driven basins in the northern Rocky Mountains. Red data points from Mueller and Pitlick *[2013]; blue data points from this study.*

The results of the analysis from *Mueller and Pitlick* [2013] indicate that there is a linear relationship, with about one order of magnitude scatter, where annual yield is approximately $2x10^6$ times greater than the instantaneous bankfull transport rate. The yields estimated from the 2014 transport data from FR1 and FR 2 of Fall River fall within the upper 33% of this dataset. However, rivers with similar physical characteristics to Fall River are typically found in the lower third of the dataset, emphasizing the intensity of transport following the 2013 floods.

An earlier study on Fall River by *Pitlick* [1993] provides a unique opportunity to compare annual sediment loads after the Lawn Lake Flood to sediment loads following the 2013 flood, providing an historical context for the magnitude and impact of this flood. To compare the loads from this study with the earlier study, the raw data collected by Pitlick from 1983 to 1987 is re-evaluated using the shear-stress based relations developed here, generating another set of annual sediment loads for FR 1 and FR 2 in each year data were available. The annual sediment loads, along with total flow for the season, are summarized in Table (4.1) and Figure (4.3) for 1983 to 1987 and 2014.

Table 4.1. Annual Sediment Loads (Mg) from Pitlick [1993] and 2014 Using Discharge- and Shear Stress-Based Empirical Sediment Transport Relations

		1983	1984	1985	1986	1987	2014
Discharge-Based Relation	FR 1	15,500	5,900	3,100	1,500	400	1,570
	FR 2	*	9,800	6,900	8,700	5,000	3,640
Shear Stress-Based Relation	FR 1	22,218	6,196	3,871	3,210	1,342	3,008
	FR 2	*	11,720	7,368	10,080	5,085	4,648
Total Flow (cubic meters)	FR 1	4.37e7	3.74e7	2.46e7	3.64e7	1.98e7	3.20e7
	FR 2	*	4.30e7	2.83e7	3.89e7	2.37e7	4.06e7

*Insufficient data recorded in 1983 for FR 2, thus no empirical relation was created.

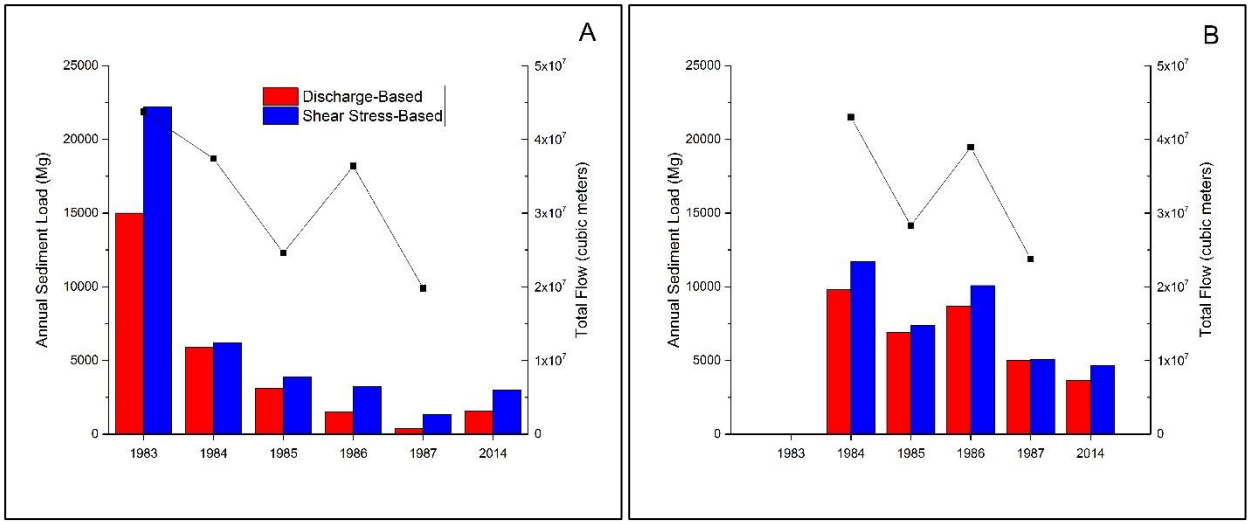

Figure 4.3. Comparison of annual sediment loads calculated from discharge-based and shear stress-based empirical sediment transport equations for a) FR 1 and b) FR 2. Years of loads calculated: 1983 (FR 1 only), 1984, 1985, 1986, 1987, and 2014. Black lines show variation in total cumulative flow for each year available.

Overall, the results of these calculations show the agreement between calculated loads in each year, and at each site. At FR 1, estimates show the same exponential decrease in total loads from 1983 to 1987 due to the diminishing supply from Roaring River, with the shear stress-based empirical relations consistently estimating higher loads than the discharge-based relations. The largest difference in loads (~43%) occurs in 1983 at FR 1. Due to high shear stresses, the largest sediment supply and hydrograph, and the nonlinearity of the relation, the shear stress-based estimate is ~6,700 Mg higher than the discharge-based estimate. At FR 2, the shear stress-based approach again consistently estimates higher loads than the discharge-based approach, showing persistent sediment transport through 1987. The fluctuation of sediment loads matches the variation in total flow in these years, regardless of approach.

Based on these shear stress empirical relations, 2014 annual sediment load values were most similar to 1986 at FR 1, with a difference of 200 Mg. Due to an exponential decline in annual sediment loads from 1983 to 1987, *Pitlick* [1993] concluded that transport rates at FR 1 had nearly recovered to pre-flood levels by 1987. During the falling limb of the 2014 hydrograph

at FR 1, transport rates declined as supply diminished. Given that Fall River was nearly recovered from an event eight times greater than the 500-year flood in five years, it is reasonable to expect a much shorter recovery time from an event approximating the 100-year flood. At FR 2, the annual sediment loads calculated in 2014 are similar to the 1987 loads, with a difference of 400 Mg. *Pitlick* [1993] observed sustained, high sediment loads through 1987 at the downstream sampling site. Observations near FR 2 indicate that fine gravel- and sand-sized sediment persisted on the bed surface throughout 2014, with significant transport rates occurring later into the season compared to upstream reaches. As was the case in the 1980s, the persistent sediment supply in 2014 was due to erosion and sediment transport from upstream reaches.

Downstream differences in sediment loads, such as we observed between FR 1 to FR 2, appear to be common in rivers where the sediment supply originates from a point source or localized area of a drainage basin. Madej and Ozaki [2009] documented similar results along Redwood Creek in California, attributing the longitudinal differences in response to timing of peak aggradation. Wohl and Cenderelli [2000] found very similar responses in upstream and downstream sites following sediment releases from Halligan Reservoir on the North Fork Poudre River. They attributed differences in sediment transport rates between upstream and downstream sites to the grain size of the material being transported and the timing of peak transport in relation to the hydrograph. Like Fall River, the same progressive movement of sediment and quicker recovery of upstream reaches was observed.

Dam removals provide examples analogous to the events experienced by Fall River. In 2011, the Condit Dam on White Salmon River in Washington was rapidly breached, eroding more than 60% of the sediment previously trapped behind the dam in 15 weeks [*Wilcox et al.*, 2014]. Studying the response of White Salmon River, *Wilcox et al.* found that the initial influx of

sediment as a result of the breach caused 1-2 m of aggradation downstream. This aggradation was completely removed in 5 days as a consequence of diminished sediment supply. The composition of transported sediment was primarily sand, which inhibited armoring during incision much like what was observed on Fall River. *Major et al.* [2012] observed the response of the Sandy River in Oregon following the 2007 breaching of a temporary dam during removal of the Marmot Dam. There they found similar results to Condit Dam, with up to 4 m of aggradation occurring in the 2 km downstream of the dam breach. Recently, the phased, large-scale dam removals on the Elwha River provided an excellent opportunity to track sediment transport for a major event, exposing about 21 million m^3 of sediment stored in a pair of reservoirs. *Warrick et al.* [2015] calculated sediment budgets for the first two years of the project, which indicated that about 65% of the stored sediment was passed through Elwha River during this time. The study also found that sediment travelled in a pulse-like fashion downstream following dam removal, resulting in aggradation on the order of ~1 m in much of the river, reducing surface grain size by a factor of 16, and depositing 2.2 million m^3 of sand and gravel offshore of the river mouth. According to the data collected, Elwha River has a higher rate of erosion of stored sediment as a percent of storage than other smaller dam removals, a result of the steep, high-energy nature of this stream [Warrick et al., 2015].

The results from this study indicate that Fall River behaves similar to streams and rivers experiencing sudden sediment inputs, but the question remains: Can we expect Fall River to respond to future events in the same way it did in 2014, or in the years following the Lawn Lake flood? Clearly, this depends on the severity of future hydrologic events, but also on the continued instability of sediment within Roaring River, which should be a concern for Park management. Given the observations and information about Fall River's past adjustments to

increased sediment supply it would be reasonable to conclude that this river is exceptionally 'resilient". However, if the sediment supply from Roaring River was to increase significantly in the future, could we expect Fall River to continue to resist major geomorphic change?

One primary reason for Fall River's ability to resist change to large increases in sediment supply is its boundary conditions. Eaton and Church [2009] found that if banks are non-erodible, a river will primarily adjust bed elevation, and channel gradient in the long-term, or bed surface texture. Especially in downstream regions, Fall River changes geomorphically in the short-term by bed aggradation, but its cohesive, vegetated banks prevent channel widening over the long term. The extent of the resistance of the channel is well-represented by the series of images from the US Geologic Survey (Figure 4.4), showing no significant change in channel pattern in a span of two and a half decades.

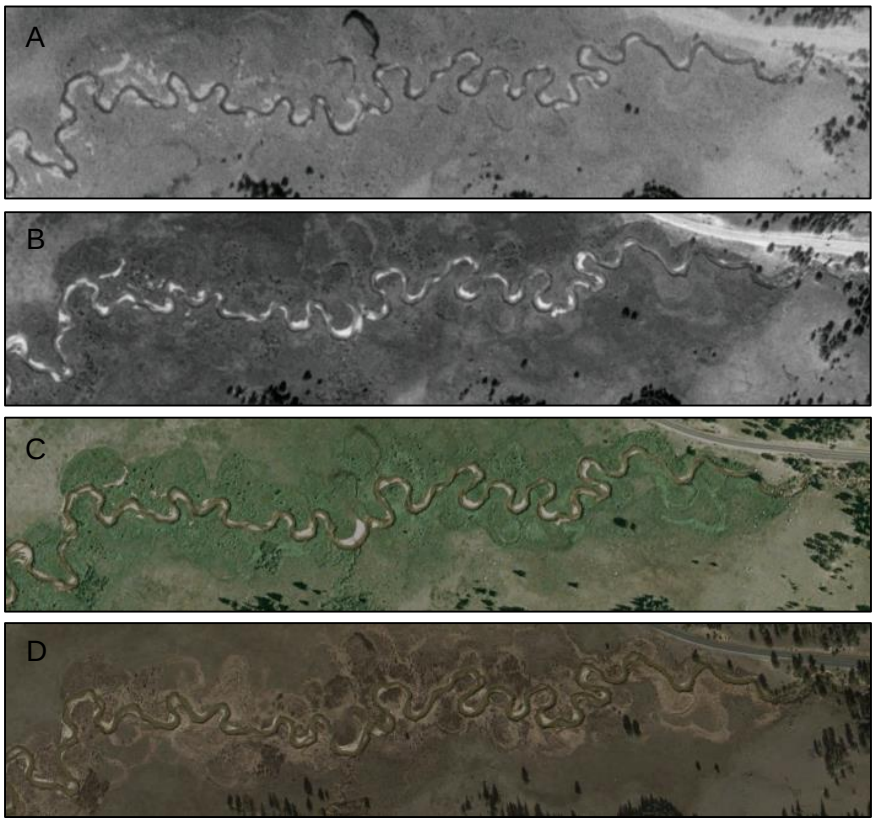

Figure 4.4. Aerial photographs of the downstream reaches of Fall River within the study area. Photographs taken by US Geologic Survey in a) 1990, b) 1999, c) 2005, and d) 2013.

Fall River exhibits the characteristics of a river which adjusts bed surface texture to accommodate sediment supply. Calculating the transport stage at bankfull conditions at FR 1 and FR 2 demonstrates the effect of decreasing grain size on the capacity for sediment transport, resulting in values of 1.7 and 2.4 for FR 1 and FR 2, respectively. The higher ratio at FR 2 supports the result that much more sediment was transported downstream where supply was greater. These spatial differences in transport in Fall River are shown by the sediment graphs for FR 1 and FR 2 (Figure 4.5). In comparison to FR 1, these graphs show that FR 2 transport rates were both much higher than and more frequently exceeding their reference transport rate.

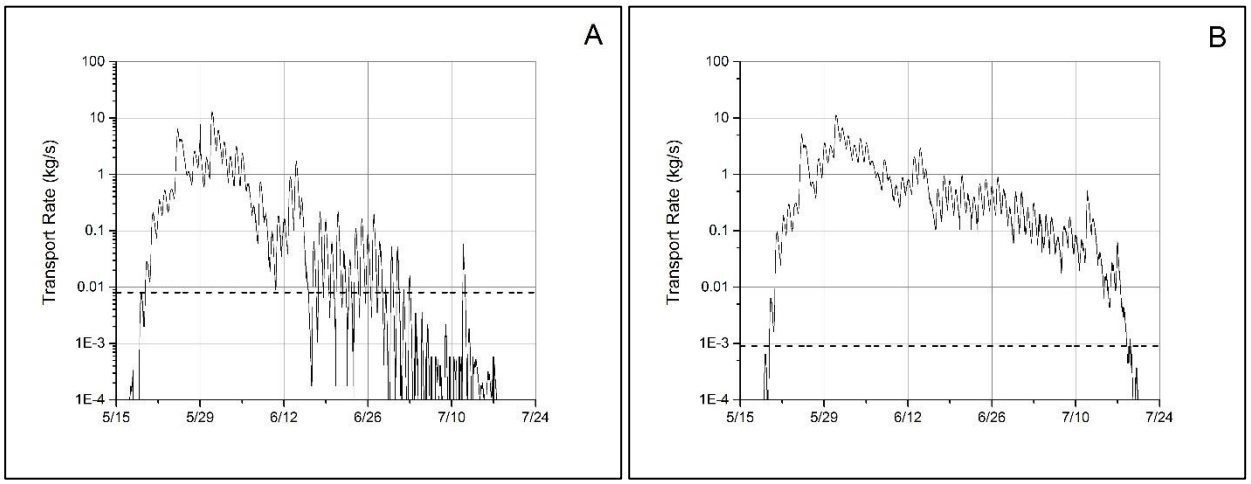

Figure 4.5. Sediment graphs showing variation in sediment transport rate (kg/s) with time in 2014 at a) FR 1, and b) FR 2. Dashed lines represent reference transport rates of 0.008 and 0.0009 kg/s for FR 1 and FR 2, respectively.

Conclusions

Downstream channel morphology in Fall River varied systematically, resulting in constant bankfull Shields stress across the study area. Sediment was found to be entrained at the same Shields stress at the three sampling sites spanning the study area. From sampling data, annual sediment loads were estimated and found to compare favorably to a geomorphic sediment budget. A comparison of these values with data from five years following the Lawn Lake flood indicates that 2014 sediment loads were similar to the loads in the last two years of that study.

Fall River's channel morphology was not substantially changed by the 2013 flood, resulting primarily in erosion of sediment deposited during the flood. The cohesive banks along Fall River's channel prevented bank erosion and significant change in channel width. A majority of the sediment load was accommodated by an adjustment of bed surface texture, especially in upstream reaches.

The comparison of loads immediately following the 2013 flood to loads several years after the 1982 Lawn Lake Flood, as well as observations of geomorphic response after each event, indicate that Fall River responded similarly to each event, relative to its magnitude. While the response differed in between upstream and downstream reaches, Fall River remains highly resistant to significant geomorphic changes. Despite instability in the Roaring River channel which will continue to supply sediment indefinitely, these increases in sediment inputs during significant events are not sufficient to geomorphically change Fall River's highly resistant channel.

REFERENCES

Abderrezzak, K.E.K., and A. Paquier (2011), Applicability of Sediment Transport Capacity Formulas to Dam-Break Flows over Movable Beds, *Journal of Hydraulic Engineering, 137 (2),* 209-221.

Baker, V.R., (1977), Stream-channel response to floods, with examples from central Texas, *Geologic Society of America Bulletin, 88 (8),* 1057-1071.

Cenderelli, D.A., and E.E. Wohl (2001), Peak discharge estimates of glacial-lake outburst floods and "normal" climatic floods in the Mount Everest region, Nepal. *Geomorphology, 40,* 57-90.

Cenderelli, D.A., and E.E. Wohl (2003), Flow hydraulics and geomorphic effects of the glacial-lake outburst floods in the Mount Everest region, Nepal, *Earth Surface Processes and Landforms, 28,* 385-407.

Clayton, J.A., and J. Pitlick (2007), Spatial and temporal variations in bed load transport intensity in a gravel bed river bend, *Water Resources Research, 43 (2),* 13 pp.

Cole, J.C., and W.A. Braddock (2008), Geologic map of Estes Park 30' x 60' quadrangle, North-Central Colorado. *Scientific Investigations Map,* U.S. Geological Survey, Denver, Colorado.

Costa, J.E., and J.E. O'Connor (1995), Geomorphically effective floods, *American Geophysical Union Monograph, 89,* 45-56.

Cui, Y., (2000), Numerical Modelling of Sediment Transport in the Sandy River, OR Following Removal of Marmot Dam, *Technical Report,* 86 pp., Stillwater Sciences, Berkeley, California.

Dietrich, W.E., Kirchner, J.W., Ikeda, H., and F. Iseya (1989), Sediment supply and the development of the coarse surface layer in gravel-bedded rivers, *Nature, 340,* 215-270.

Eaton, B.C., and M. Church (2004), A graded stream response relation for bed-load dominated streams, *Journal of Geophysical Research, 109,* 18 pp.

Eaton, B.C., and M. Church (2009), Channel stability in bed load-dominated streams with nonerodible banks: inferences from experiments in a sinuous flume, *Journal of Geophysical Research, 114,* 17 pp.

Erwin, S.O., Schmidt, J.C., and N.C. Nelson (2011), Downstream effects of impounding a natural lake: the Snake River downstream from Jackson Lake Dam, Wyoming, USA, *Earth Surface Processes and Landforms, 36,* 1421-1434.

Ferguson, R.I., and P. Ashworth, (1991), Slope-induced changes in channel character along a gravel-bed stream: the Allt Dubhaig, *Earth Surface Processes and Landforms, 16,* 65-82.

Hassan, M.A., Egozi, R., and G. Parker (2006), Experiments on the effect of hydrograph characteristics on vertical grain sorting, *Water Resources Research, 42,* 15 pp.

Jarret, R.D., and J.E. Costa (1986), Hydrology, Geomorphology, and Dam-Break Modeling of the July 15, 1982, Lawn Lake Dam and Cascade Lake Dam Failures, *Professional Paper 1369*, 78 pp., U.S. Geological Survey, Larimer County, Colorado.

Kuhnle, R.A., (1989), Bed-surface size changes in gravel-bed channel, *Journal of Hydraulic Engineering, 115 (6)*, 731-743.

Lapointe, M.F., Secretan, Y., Driscoll, S.N., Bergeron, N., and M. Leclerc (1998), Response of the Ha! Ha! River to the flood of July 1996 in the Saguenay Region of Quebec: Large-scale avulsion in a glaciated valley, *Water Resources Research, 34 (9)*, 2383-2392.

Lewicki, M., Pizzuto, J.E., Moglen, G.E., and N.E. Allmendinger (2007), A watershed scale numerical model of the impact of land use change on bed material transport in suburban Maryland, USA, *Water Resources Research*, *43*, 11 pp.

Lisle, T.E., (1981), The recovery of aggraded stream channels at gauging stations in northern California and southern Oregon. Erosion and Sediment Transport in Pacific Rim Steeplands, *Publication No. 132*, 12 pp., International Association Hydrological Sciences, Arcata, California.

Madej, M.A., and V. Ozaki, (2009), Persistence of effects of high sediment loading in a salmon-bearing river, northern California, *Geologic Society of America, Special Paper 451*, 43 pp.

Major, J.J., O'Connor, J.E., Podolak, C.J., Keith, M.K., Grant, G.E., Spicer, K.R., Pittman, S., Bragg, H.M., Wallick, J.R., Tanner, D.Q., Rhode, A., and P.R. Wilcock, (2012), Geomorphic response of the Sandy River, Oregon, to removal of Marmot Dam. *U.S. Geological Survey, Professional Paper 1792*, 76 pp.

Mueller, E.R., and J. Pitlick (2013), Sediment supply and channel morphology in mountain river systems: 1. Relative importance of lithology, topography, and climate, *Journal of Geophysical Research: Earth Surface, 118*, 2325-2342.

Meyer-Peter, E., and R. Müller (1948), Formulas for bed-load transport, *Proceedings 2nd Congress*, 25 pp., International Association of Hydraulic Research, Stockholm, Sweden.

NRCS-NWCC, Snotel monthly and annual precipitation data at Willow Park, Version 1.3, October 1981 to September 2014, http://www.wcc.nrcs.usda.gov/reportGenerator, Natural Resources Conservation Service, Denver, Colorado. (Updated daily.)

Parker, G., (1979), Hydraulic geometry of active gravel rivers, *Journal of the Hydraulics Division, 105 (9)*, 1185-1201.

Parker, G., (1990), Surface-based bedload transport relation for gravel rivers, *Journal of Hydraulic Research, 28 (4)*, 417-436.

Parker, G., Klingeman, P.C., and McLean, D.G. (1982), Bedload and size distribution in paved gravel-bed streams. *Journal of the Hydraulics Division*, *108 (4)*, 544-571.

Pitlick, J., (1993), Response and recovery of a subalpine stream following a catastrophic flood, *Geological Society of American Bulletin, 105*, 657-670.

Pitlick, J., (1994), Relation between peak flows, precipitation, and physiography for five mountainous regions in the western USA, *Journal of Hydrology*, *158*, 219-240.

Pitlick, J. and R. Cress, (2002), Downstream changes in the channel geometry of a large gravel bed river, *Water Resources Research, 38 (10),* 11 pp.

Pitlick, J., Marr, J., and J. Pizzuto (2013), Width adjustment in experimental gravel-bed channels in response to overbank flows, *Journal of Geophysical Research: Earth Surface, 188,* 553-570.

Pizzuto, J.E., (1992), The morphology of graded gravel rivers: a network perspective, *Geomorphology, 5,* 457-474.

Pizzuto, J. E., (1994), Channel adjustments to changing discharges, Powder River between Moorhead and Broadus, Montana, *Geologic Society of America Bulletin, 106,* 1494-1501.

Rickenmann, D., and A. Koschni, (2010), Sediment loads due to fluvial transport and debris flows during the 2005 flood events in Switzerland, *Hydrologic Processes, 24,* 993-1007.

Rathburn S.L., Rubin, Z.K., and E.E. Wohl, (2013), Evaluating channel response to and extreme sedimentation event in the context of historical range of variability: Upper Colorado River, USA, *Earth Surface Processes and Landforms, 38,* 391-406.

Segura, C., and J. Pitlick (2015), Coupling fluvial-hydraulic models to predict gravel transport in spatially variable flows, *Journal of Geophysical Research: Earth Surface, 120.*

Schumm, S.A., (1969), River metamorphosis, Journal of Hydraulic Division, 95, 255-273.

Schumm, S.A., and R.W. Lichty (1963), Channel widening and floodplain construction along Cimarron River in Southwestern Kansas, *Professional Paper 352-D,* 18 pp., U.S. Geologic Survey, Alexandria, Virginia.

Warrick, J.A., Bountry, J.A., East, A.E., Magirl, C.S., Randle, T.J., Gelfenbaum, G., Ritchie, A.C., Pess, G.R., Leung, V., and J.J. Duda, (2015), Large-scale dam removal on the Elwha River, Washington, USA: source-to-sink sediment budget and analysis. *Geomorphology, In Press,* 22 pp.

Wilcock, P.R., Kenworthy, S.T., and J.C. Crowe (2001), Experimental study of the transport of mixed sand and gravel, *Water Resources Research, 37 (12),* 3349-3358.

Wilcox, A.C., O'Connor, J.E., and J.J. Major, (2014), Rapid reservoir erosion, hyperconcentrated flow, and downstream deposition triggered by breaching of 38-m Condit Dam, White Salmon River, Washington. *Journal of Geophysical Research: Earth Surface, 119 (6),* 1376-1394.

Wohl, E.E. and Cenderelli, D.A., (2000), Sediment deposition and transport patterns following a reservoir sediment release. *Water Resources Research, 36 (1),* 319-333.

Yochum, S.E., and D.S. Moore (2013), Colorado Front Range Flood of 2013: Peak flow estimates at selected mountain stream locations, 44 pp., USDA Natural Resources Conservation Service, Denver, Colorado.

APPENDIX A

Downstream Trends

Cross Section	Dist DS (m)	Area (m^2)	Width (m)	Mean Depth (m)	Mean Bed Elevation (m)	$D50_{surf}$ (mm)	$D84_{surf}$ (mm)	$D50_{sub}$ (mm)	$D84_{sub}$ (mm)
XS 0	0.0	4.1	8.6	0.5	2591.42	61.8	107.6	5.0	36.0
XS 1	111.6	21.0	17.3	1.2	2590.47				
XS 2	206.5	5.2	9.0	0.6	2589.45				
XS 3	306.6	10.7	16.0	0.7	2589.20	48.8	96.3	5.01	26.5
XS 4	396.5	12.9	13.6	1.0	2588.65				
XS 5	506.1	15.6	21.0	0.8	2588.08	43.4	83.6	13.9	37.7
XS 6	609.0	6.9	14.6	0.5	2587.49				
XS 7	714.3	7.0	19.0	0.4	2587.20	48.9	87.1	8.6	32.3
XS 8	817.3	4.2	10.0	0.4	2586.28				
XS 9	906.8	6.5	11.2	0.6	2585.82	33.9	64.0	17.3	39.0
XS 10	1005.5	5.5	11.3	0.5	2585.17				
XS 11	1114.1	8.6	8.1	1.1	2584.50	22.2	42.7	6.6	21.3
XS 12	1212.5	10.8	12.0	0.9	2584.44				
XS 13	1296.3	4.5	10.0	0.5	2583.97	22.4	37.6	5.8	19.0
FR 1	1389.8	8.0	14.1	0.6	2583.66	21.4	37.6	3.2	21.4
XS 14	1399.0	11.7	17.0	0.7	2583.76	17.8	35.2	12.5	42.7
XS 15	1491.6	10.4	16.0	0.7	2583.54				
XS 16	1582.4	4.2	8.3	0.5	2582.66	19.0	42.4	6.3	20.6
XS 17	1688.0	10.3	12.0	0.9	2582.49				
XS 18	1809.1	10.1	14.9	0.7	2581.98	19.0	39.7	19.0	48.4
XS 19	1911.7	11.6	9.5	1.2	2581.50				
XS 20	2025.0	14.0	10.5	1.3	2580.99	20.6	37.2	16.7	37.1
XS 21	2133.6	7.5	11.2	0.7	2580.92				
XS 22	2235.4	8.5	11.2	0.8	2580.59	21.0	39.5	13.1	36.6
XS 23	2343.1	10.8	20.0	0.5	2580.49				
XS 24	2440.3	7.2	10.4	0.7	2579.82				
XS 25	2534.9	7.7	9.5	0.8	2579.82	18.4	29.9	4.2	16.5
XS 26	2639.4	8.9	11.0	0.8	2579.25				
XS 27	2736.2	10.3	12.0	0.9	2579.01				
XS 28	2849.0	12.5	15.5	0.8	2578.93	15.7	25.1	5.7	11.7
XS 29	2940.2	14.4	15.0	1.0	2578.62				
XS 30	3065.8	8.3	11.4	0.7	2578.32				
XS 31	3166.6	9.9	12.0	0.8	2577.99	13.3	23.3	7.4	14.2

Cross Section	Dist DS (m)	Area (m^2)	Width (m)	Mean Depth (m)	Mean Bed Elevation (m)	$D50_{surf}$ (mm)	$D84_{surf}$ (mm)	$D50_{sub}$ (mm)	$D84_{sub}$ (mm)
XS 32	3248.2	9.8	17.0	0.6	2578.14				
XS 33	3391.2	9.4	14.8	0.6	2577.79	18.7	26.5	5.7	15.4
XS 34	3481.1	7.5	14.7	0.5	2577.60				
XS 35	3614.7	10.5	30.0	0.4	2577.60	9.7	30.2	1.5	3.6
XS 36	3708.7	9.1	13.0	0.7	2577.23				
XS 37	3816.2	8.3	10.3	0.8	2576.88	18.5	30.5	1.5	6.5
XS 38	3919.9	8.9	14.0	0.6	2576.84				
XS 39	4037.8	6.7	10.5	0.6	2576.58	13.5	22.3	1.2	11.1
XS 40	4127.1	8.6	11.0	0.8	2576.22				
XS 41	4234.5	10.0	13.5	0.7	2576.19	9.6	14.7	3.5	7.4
XS 42	4347.1	12.0	15.2	0.8	2575.93				
XS 43	4438.3	7.9	12.1	0.7	2575.87	14.6	27.6	3.4	11.1
XS 44	4539.0	9.9	11.6	0.9	2575.59				
XS 45	4622.2	8.8	8.7	1.0	2575.15	9.1	17.8	1.4	10.8
XS 46	4733.0	10.4	11.3	0.9	2575.29				
XS 47	4861.4	8.6	10.5	0.8	2575.02	7.6	12.2	2.5	4.2
XS 48	4971.3	10.3	14.5	0.7	2574.92				
XS 49	5096.0	12.1	17.7	0.7	2574.94	8.2	14.1	1.5	9.2
FR 2	5228.1	9.6	9.0	1.1	2574.20	7.7	23.9	1.3	2.0

Cross Section Surveys

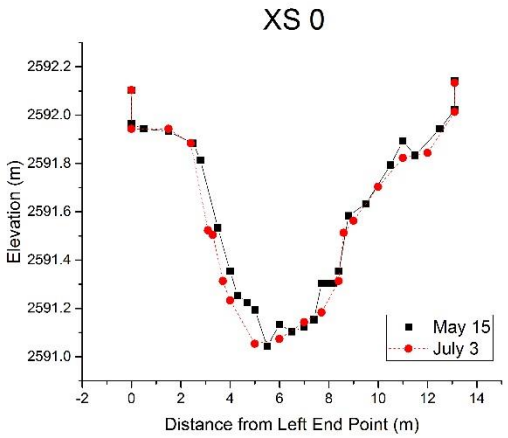

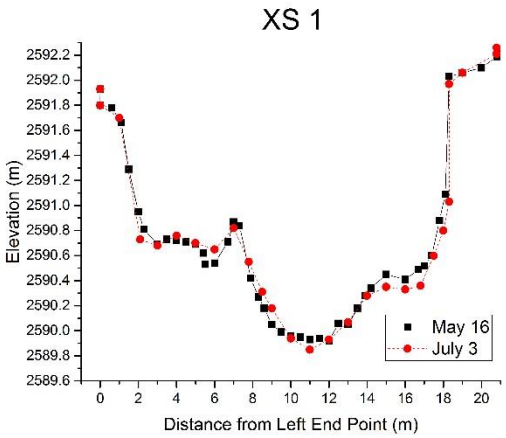

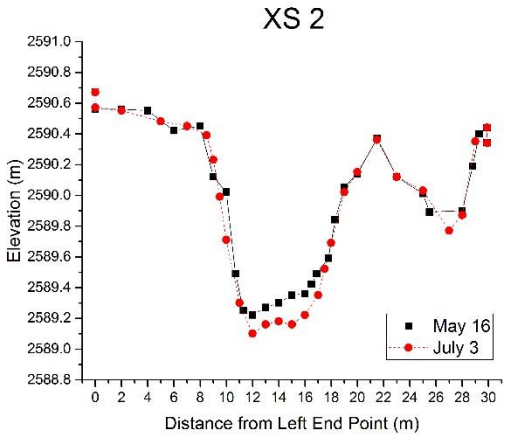

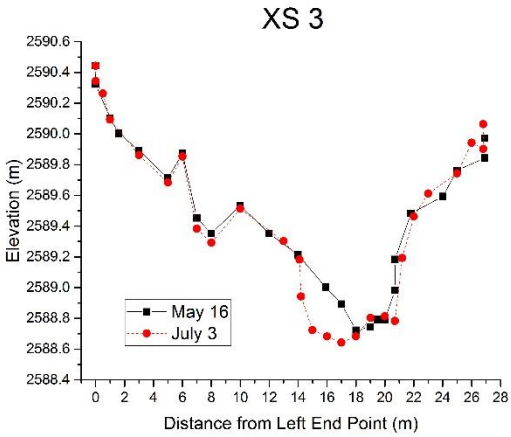

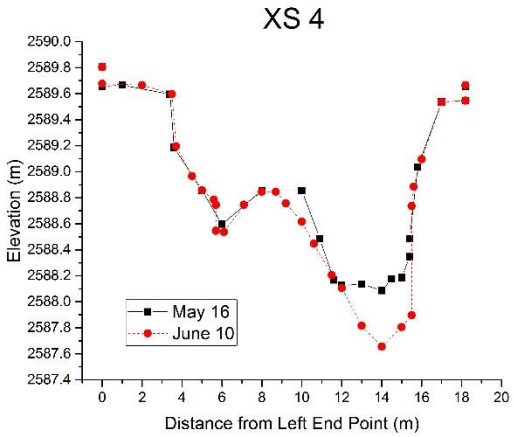

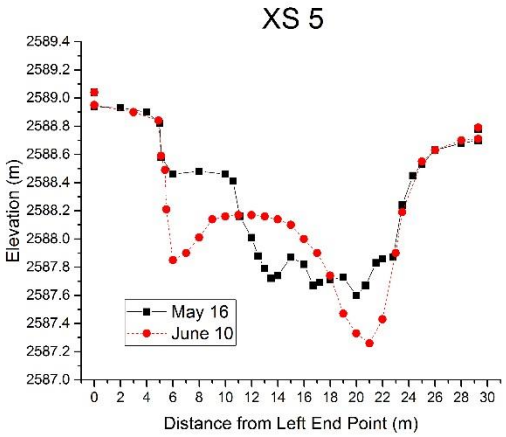

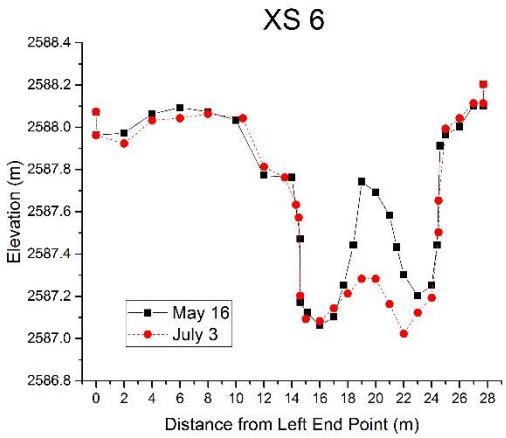
XS 6
Elevation (m)
Distance from Left End Point (m)
May 16
July 3

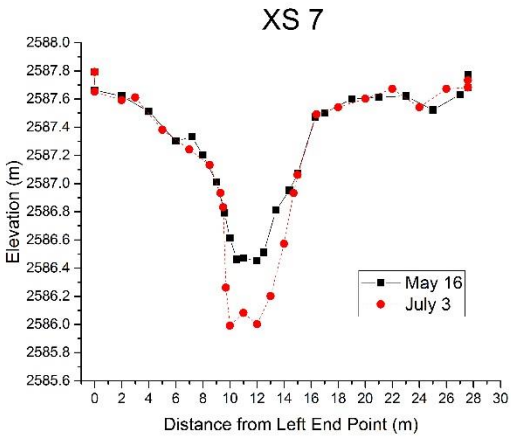
XS 7
Elevation (m)
Distance from Left End Point (m)
May 16
July 3

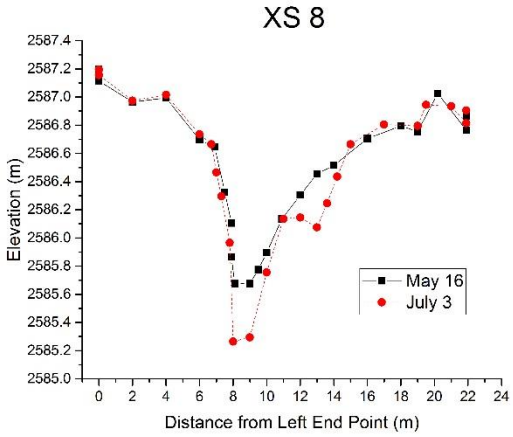
XS 8
Elevation (m)
Distance from Left End Point (m)
May 16
July 3

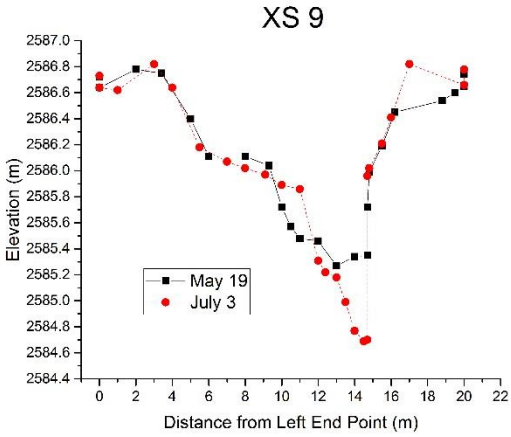
XS 9
Elevation (m)
Distance from Left End Point (m)
May 19
July 3

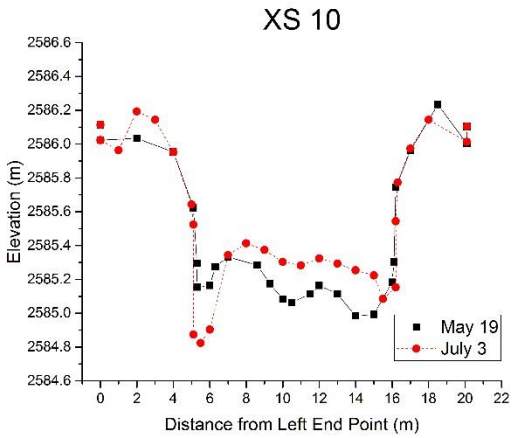
XS 10
Elevation (m)
Distance from Left End Point (m)
May 19
July 3

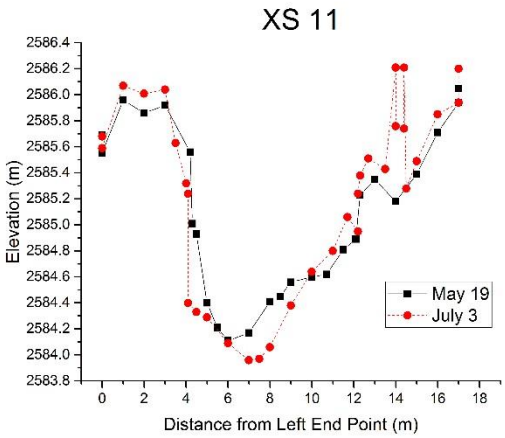
XS 11
Elevation (m)
Distance from Left End Point (m)
May 19
July 3

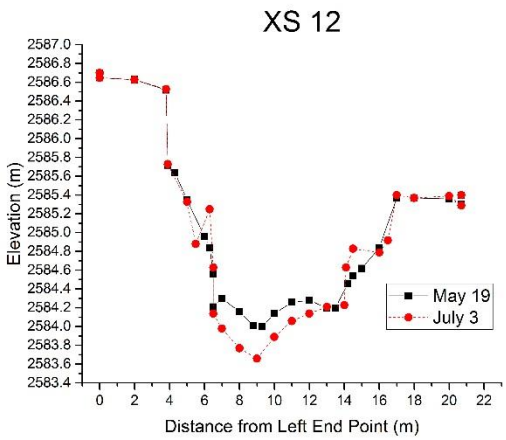
XS 12
Elevation (m)
Distance from Left End Point (m)
May 19
July 3

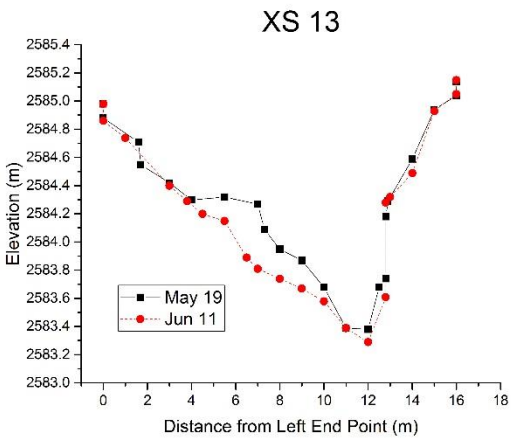
XS 13
Elevation (m)
Distance from Left End Point (m)
May 19
Jun 11

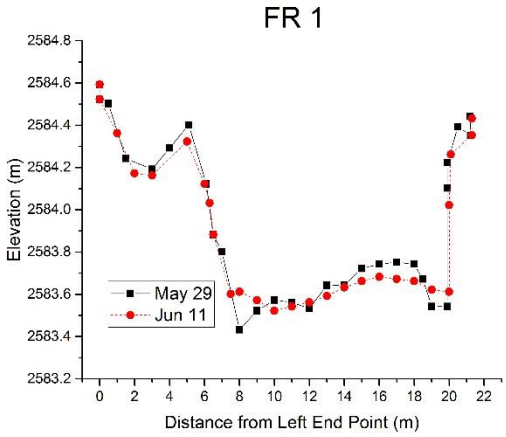
FR 1
Elevation (m)
Distance from Left End Point (m)
May 29
Jun 11

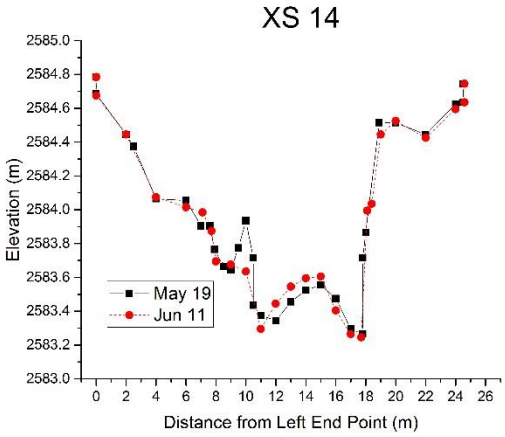
XS 14
Elevation (m)
Distance from Left End Point (m)
May 19
Jun 11

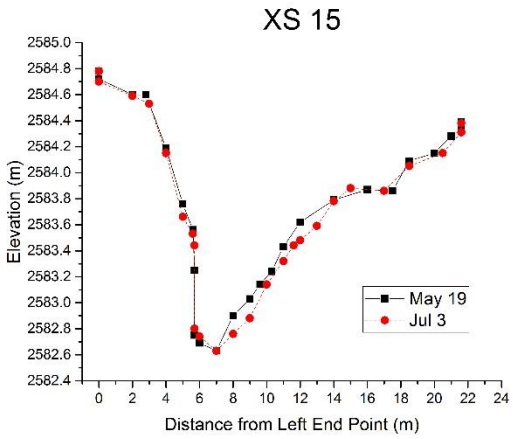
XS 15
Elevation (m)
Distance from Left End Point (m)
May 19
Jul 3

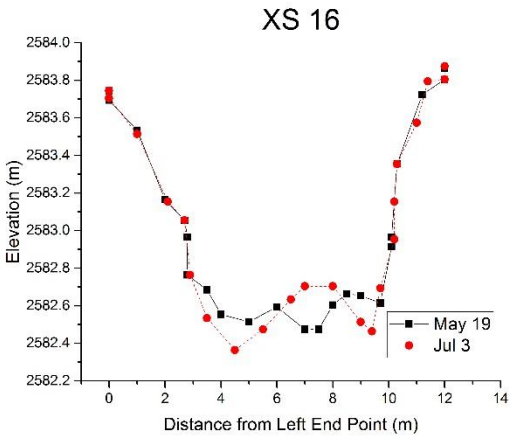
XS 16
Elevation (m)
Distance from Left End Point (m)
May 19
Jul 3

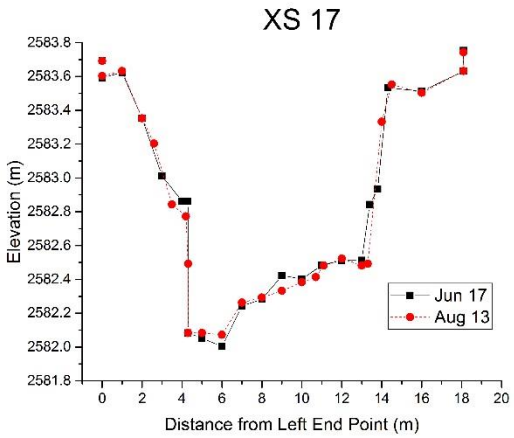
XS 17
Elevation (m)
Distance from Left End Point (m)
Jun 17
Aug 13

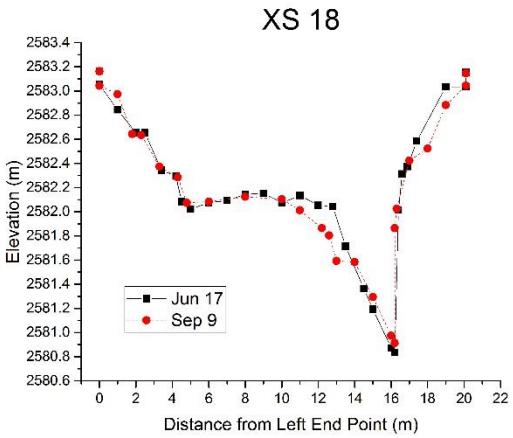
XS 18
Elevation (m)
Distance from Left End Point (m)
Jun 17
Sep 9

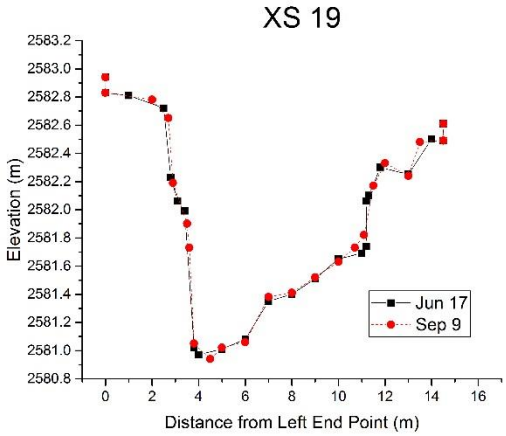
XS 19
Elevation (m)
Distance from Left End Point (m)
Jun 17
Sep 9

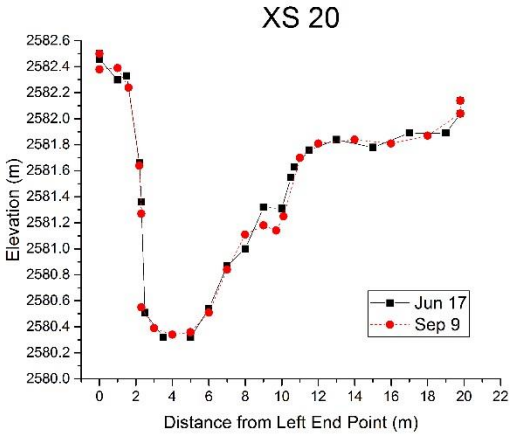
XS 20
Elevation (m)
Distance from Left End Point (m)
Jun 17
Sep 9

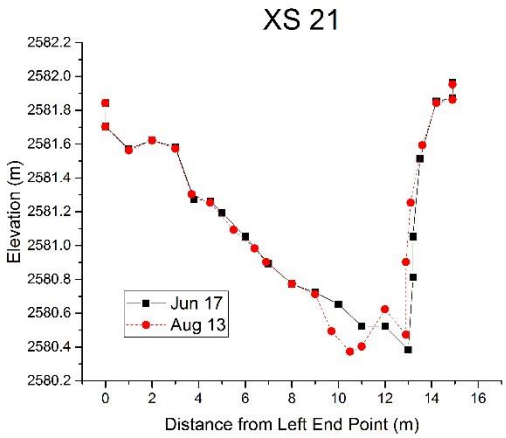
XS 21
Elevation (m)
Distance from Left End Point (m)
Jun 17
Aug 13

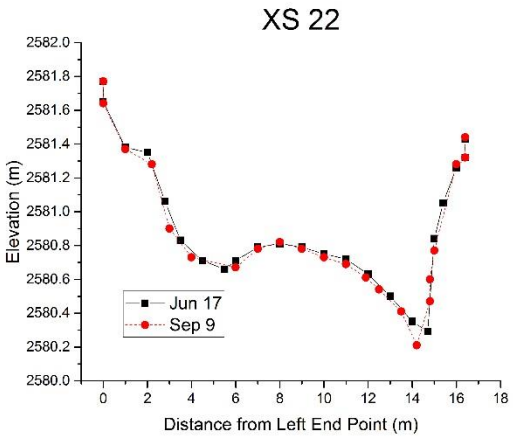
XS 22
Elevation (m)
Distance from Left End Point (m)
Jun 17
Sep 9

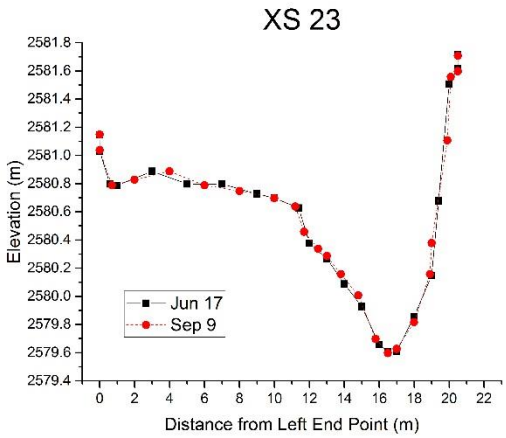
XS 23
Elevation (m)
Distance from Left End Point (m)
Jun 17
Sep 9

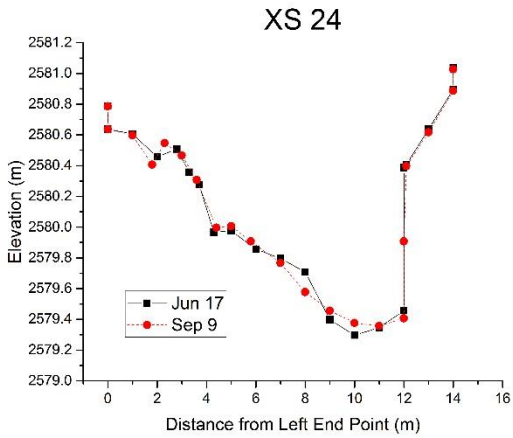
XS 24
Elevation (m)
Distance from Left End Point (m)
Jun 17
Sep 9

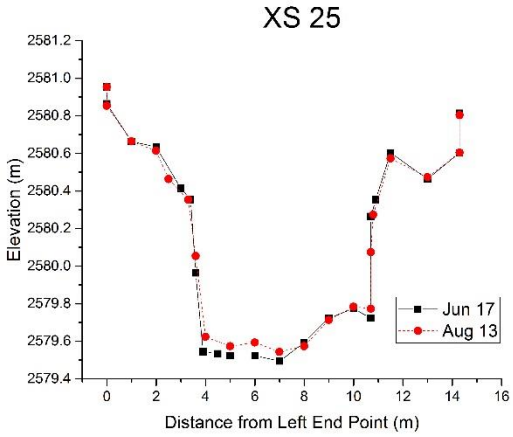
XS 25
Elevation (m)
Distance from Left End Point (m)
Jun 17
Aug 13

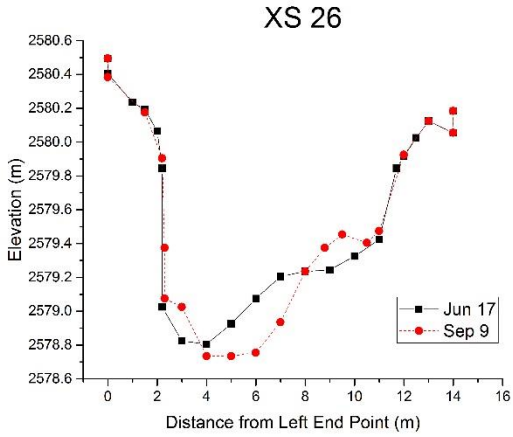
XS 26
Elevation (m)
Distance from Left End Point (m)
Jun 17
Sep 9

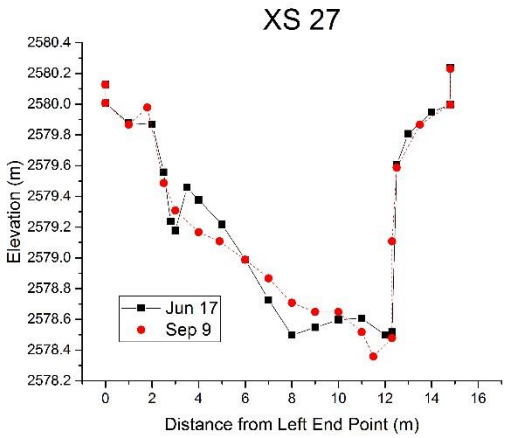
XS 27
Elevation (m)
Distance from Left End Point (m)
Jun 17
Sep 9

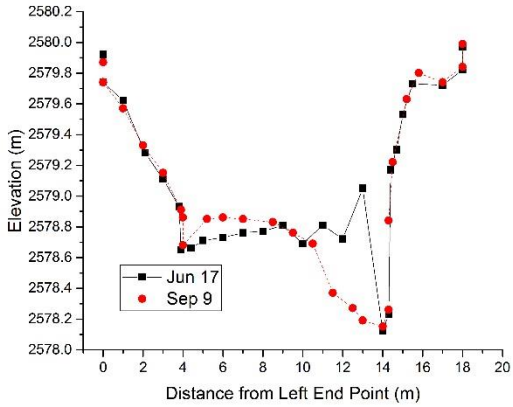
XS 28
Elevation (m)
Distance from Left End Point (m)
Jun 17
Sep 9

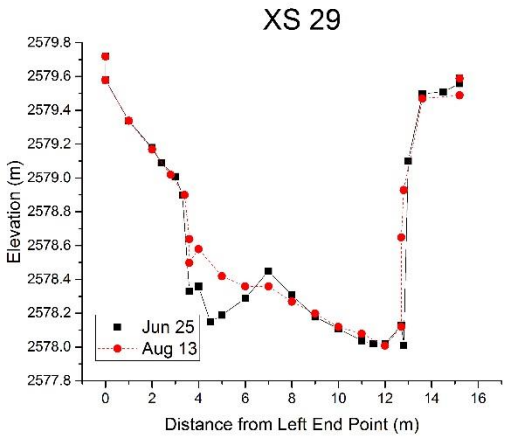
XS 29
Elevation (m)
Distance from Left End Point (m)
Jun 25
Aug 13

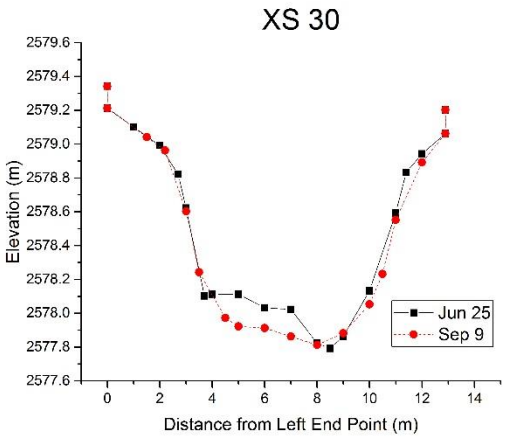
XS 30
Elevation (m)
Distance from Left End Point (m)
Jun 25
Sep 9

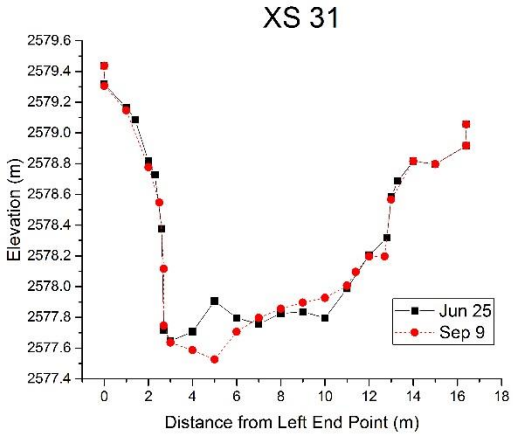
XS 31
Elevation (m)
Distance from Left End Point (m)
Jun 25
Sep 9

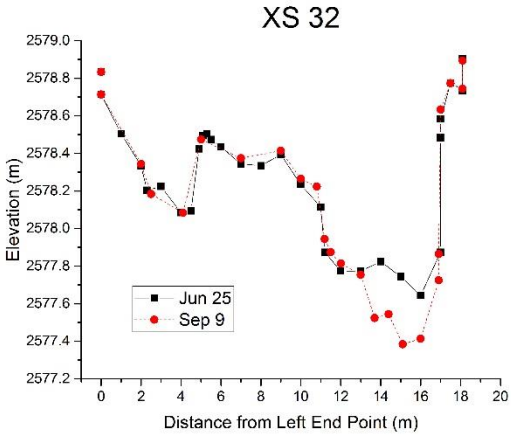
XS 32
Elevation (m)
Distance from Left End Point (m)
Jun 25
Sep 9

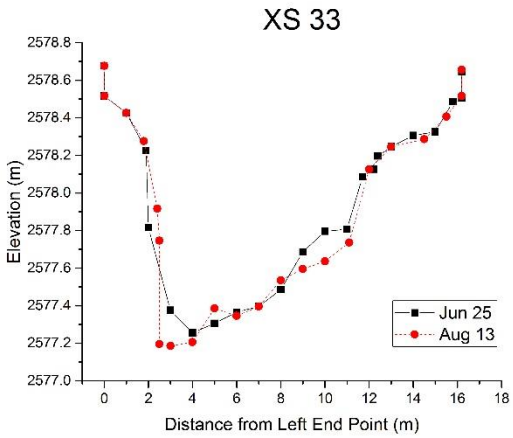
XS 33
Elevation (m)
Distance from Left End Point (m)
Jun 25
Aug 13

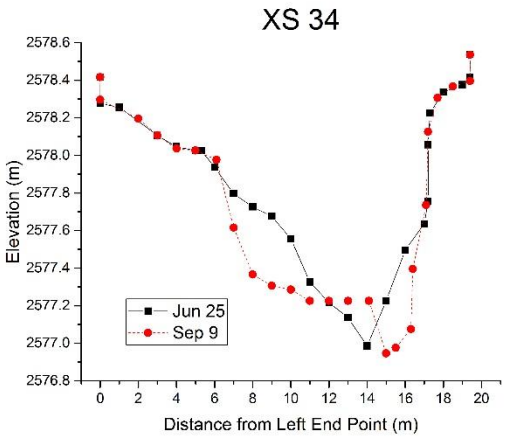
XS 34
Elevation (m)
Distance from Left End Point (m)
Jun 25
Sep 9

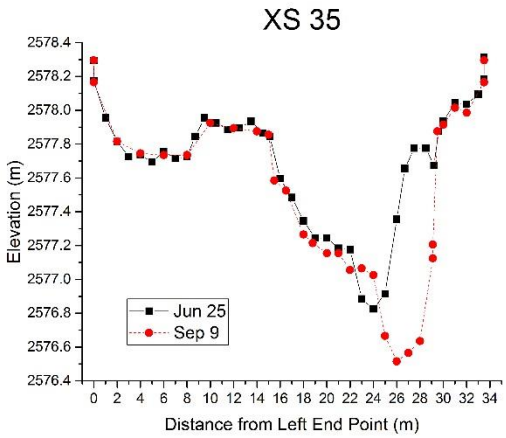
XS 35
Elevation (m)
Distance from Left End Point (m)
Jun 25
Sep 9

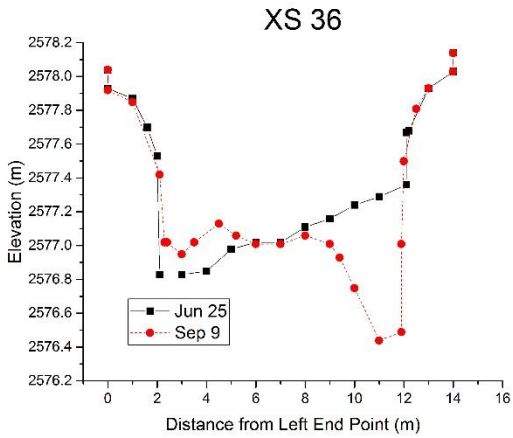
XS 36
Elevation (m)
Distance from Left End Point (m)
Jun 25
Sep 9

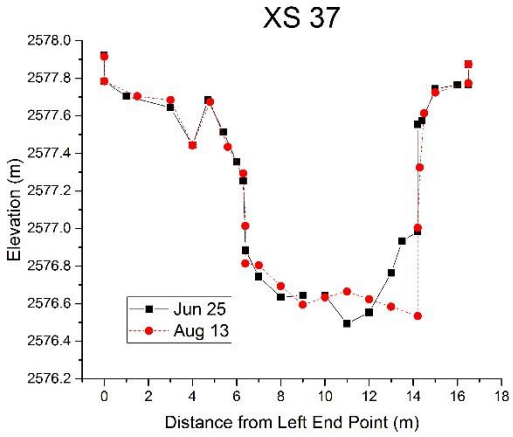
XS 37
Elevation (m)
Distance from Left End Point (m)
Jun 25
Aug 13

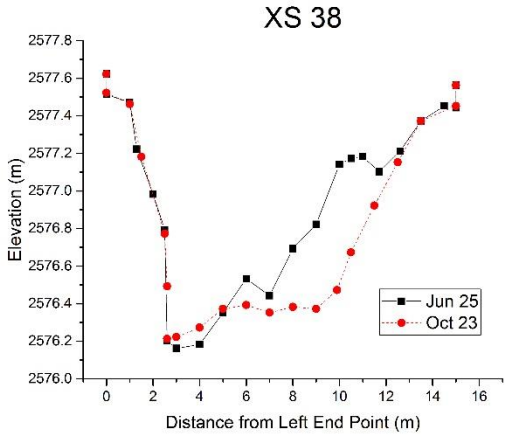
XS 38
Elevation (m)
Distance from Left End Point (m)
Jun 25
Oct 23

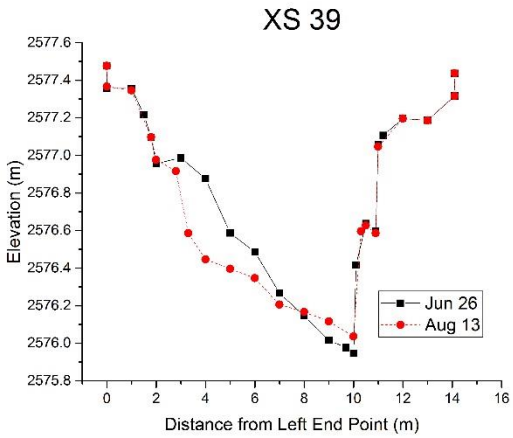
XS 39
Elevation (m)
Distance from Left End Point (m)
Jun 26
Aug 13

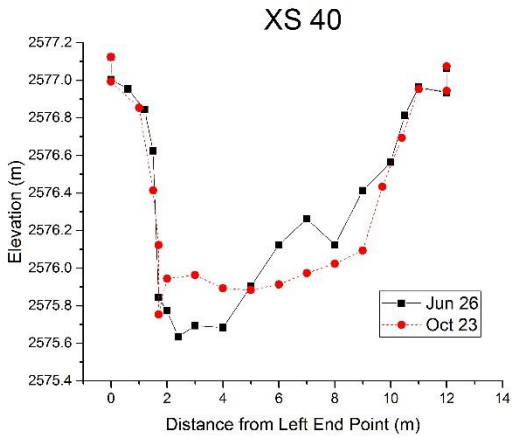
XS 40
Elevation (m)
Distance from Left End Point (m)
Jun 26
Oct 23

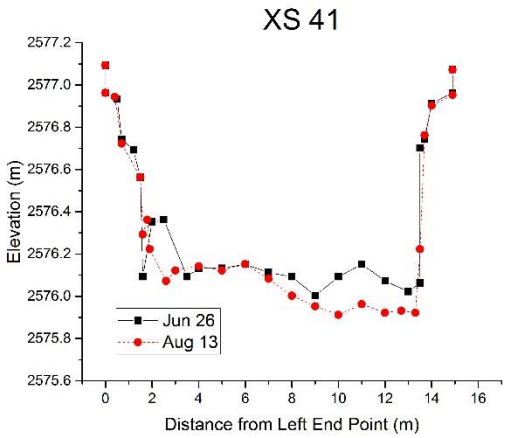
XS 41
Elevation (m)
Distance from Left End Point (m)
Jun 26
Aug 13

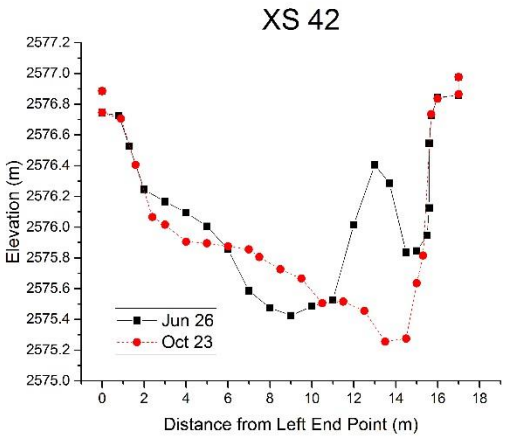
XS 42
Elevation (m)
Distance from Left End Point (m)
Jun 26
Oct 23

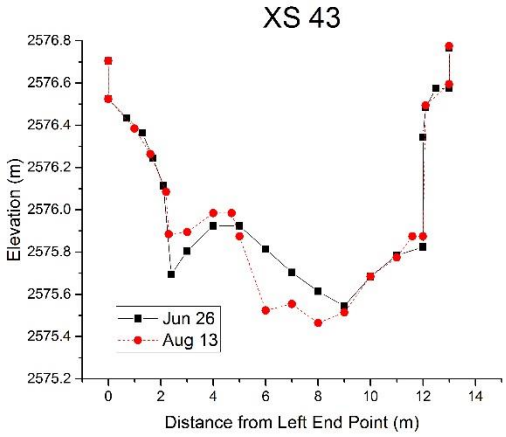
XS 43
Elevation (m)
Distance from Left End Point (m)
Jun 26
Aug 13

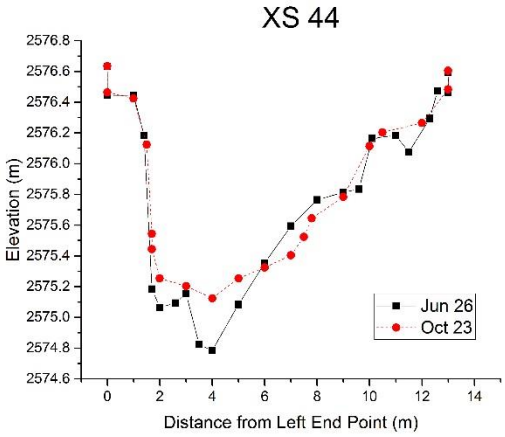
XS 44
Elevation (m)
Distance from Left End Point (m)
Jun 26
Oct 23

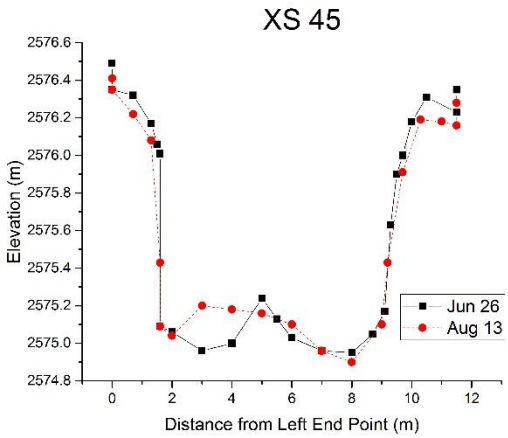
XS 45
Elevation (m)
Distance from Left End Point (m)
Jun 26
Aug 13

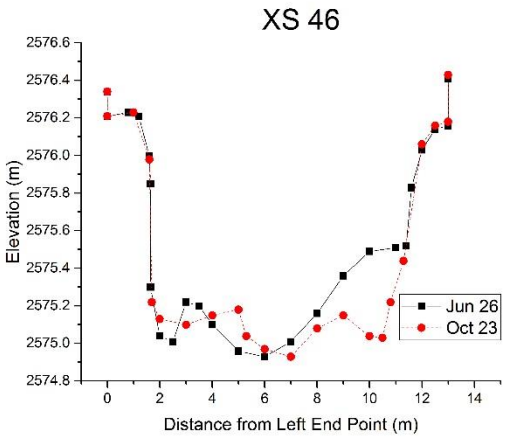
XS 46
Elevation (m)
Distance from Left End Point (m)
Jun 26
Oct 23

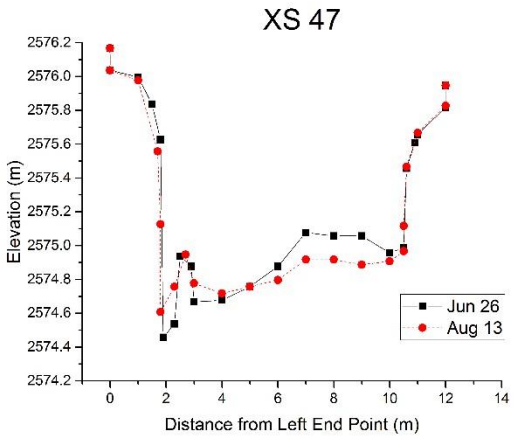
XS 47
Elevation (m)
Distance from Left End Point (m)
Jun 26
Aug 13

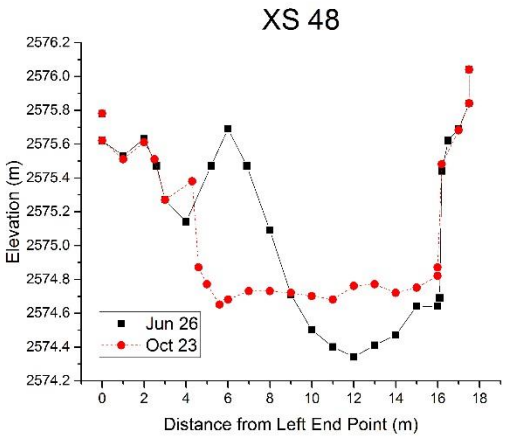
XS 48
Elevation (m)
Distance from Left End Point (m)
Jun 26
Oct 23

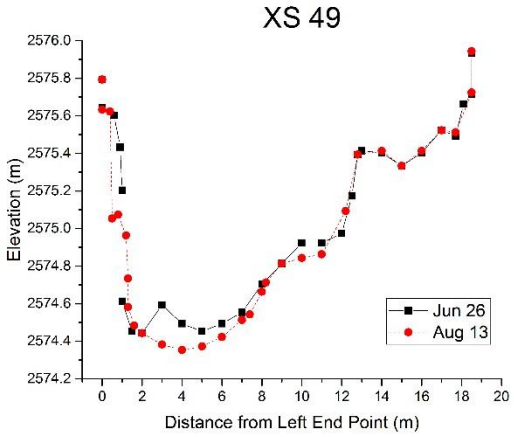
XS 49
Elevation (m)
Distance from Left End Point (m)
Jun 26
Aug 13

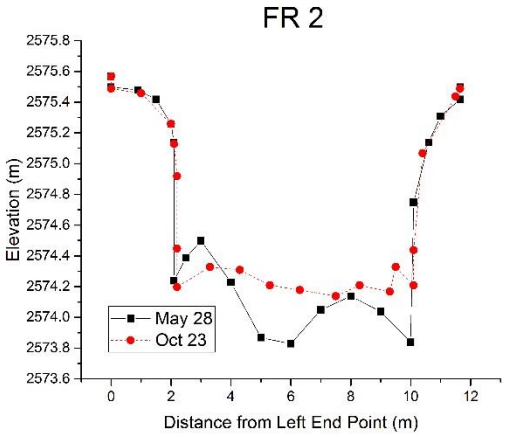
FR 2
Elevation (m)
Distance from Left End Point (m)
May 28
Oct 23

Surface Pebble Counts

Values in pebble count tables represent individual grains counted.

Pebble Count Table									
Size (mm)	XS 0	XS 3	XS 5	XS 7	XS 9	XS 11	XS 13	XS 14	XS 16
512.0	0	0	0	0	0	0	0	0	0
360.0	0	0	0	0	0	0	0	0	0
256.0	0	0	0	0	0	0	0	0	0
180.0	1	1	1	0	0	0	0	0	1
128.0	6	4	8	3	1	0	0	0	1
90.0	18	14	21	11	3	0	1	1	0
64.0	23	20	47	24	12	3	4	6	6
45.0	20	16	46	18	19	20	20	9	9
32.0	16	25	37	24	18	21	26	33	20
22.0	11	10	27	11	20	32	48	39	17
16.0	3	7	24	8	18	25	36	54	22
11.0	1	6	16	3	6	17	17	46	21
8.0	0	0	6	1	2	9	8	32	15
5.6	0	0	3	0	0	3	5	22	11
4.0	1	0	19	1	1	10	0	8	7
Pebble Count Table									
Size (mm)	XS 18	XS 20	XS 22	XS 25	XS 28	XS 31	XS 33	XS 35	XS 37
512.0	0	0	0	0	0	0	0	0	0
360.0	0	0	0	0	0	0	0	0	0
256.0	0	0	0	0	0	0	0	0	0
180.0	0	0	0	0	0	0	0	0	0
128.0	0	0	0	0	0	0	0	0	0
90.0	2	1	0	0	0	0	0	0	0
64.0	5	2	5	0	0	0	0	0	0
45.0	9	10	10	2	0	2	0	7	1
32.0	17	18	21	10	0	2	4	7	12
22.0	26	32	30	20	23	15	22	12	22
16.0	22	35	31	29	26	27	44	10	26
11.0	24	18	23	13	19	18	16	9	11
8.0	21	12	17	10	8	15	9	11	11
5.6	9	6	5	4	4	12	3	19	7
4.0	5	11	3	11	20	20	2	25	10

Pebble Count Table									
Size (mm)	XS 39	XS 41	XS 43	XS 45	XS 47	XS 49			
512.0	0	0	0	0	0	0			
360.0	0	0	0	0	0	0			
256.0	0	0	0	0	0	0			
180.0	0	0	0	0	0	0			
128.0	0	0	0	0	0	0			
90.0	0	0	0	0	0	0			
64.0	0	0	0	0	0	0			
45.0	0	0	1	0	0	0			
32.0	0	1	10	3	0	0			
22.0	15	2	16	4	0	2			
16.0	27	7	23	13	2	10			
11.0	16	24	21	14	18	11			
8.0	15	33	22	26	25	29			
5.6	13	15	10	23	35	25			
4.0	14	18	8	17	20	23			

Subsurface Grain Size Distributions

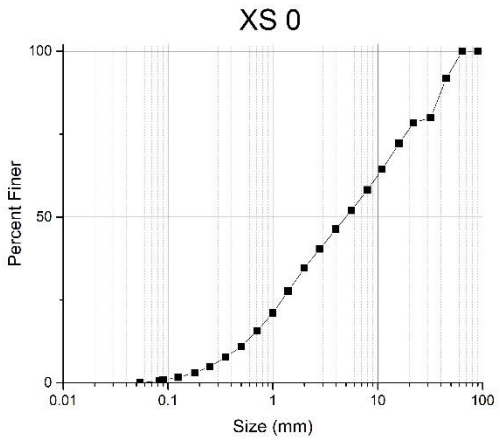

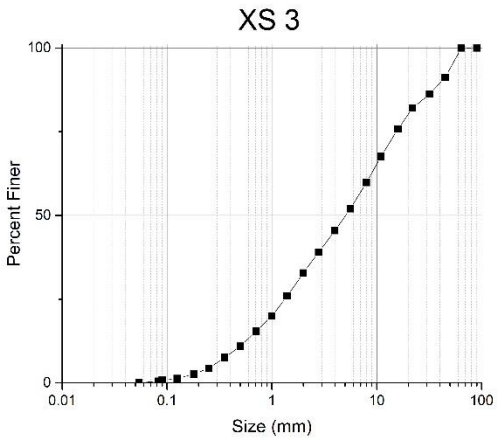

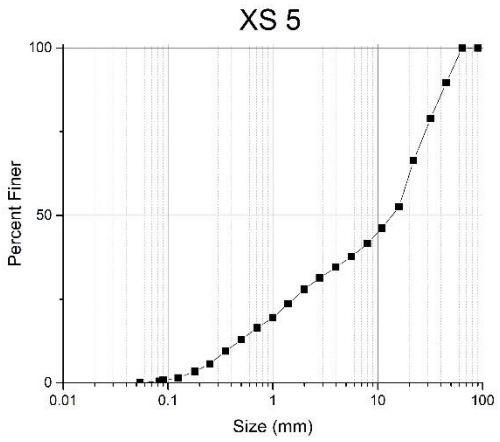

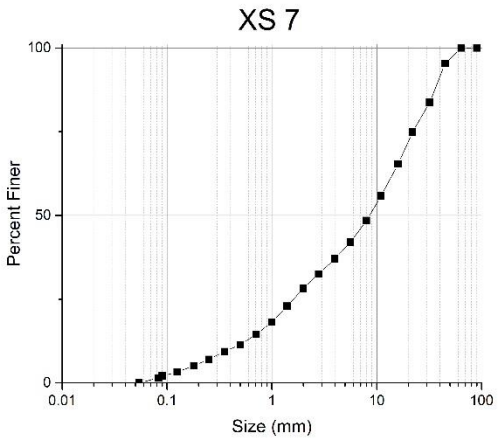

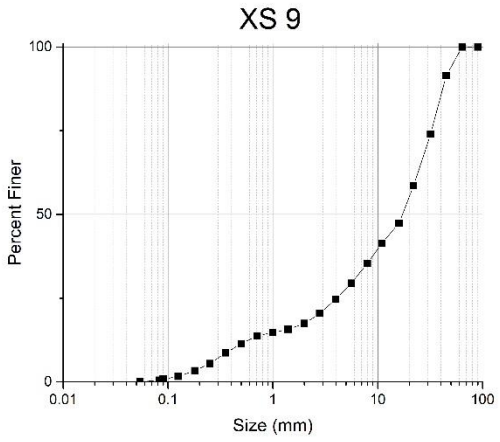

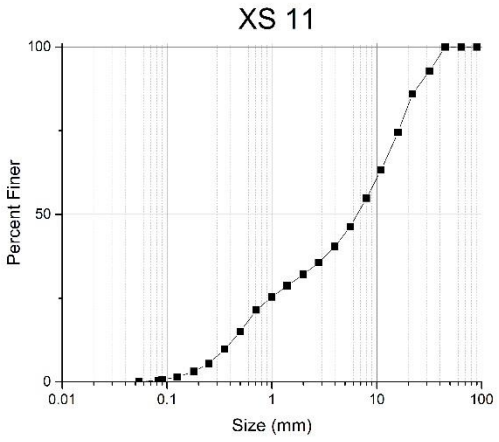

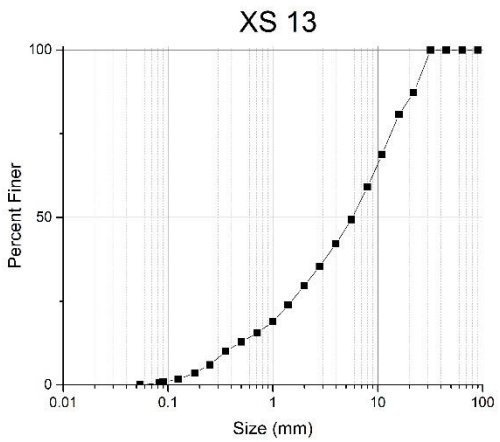
XS 13
Percent Finer
Size (mm)
100
50
0
0.01
0.1
1
10
100

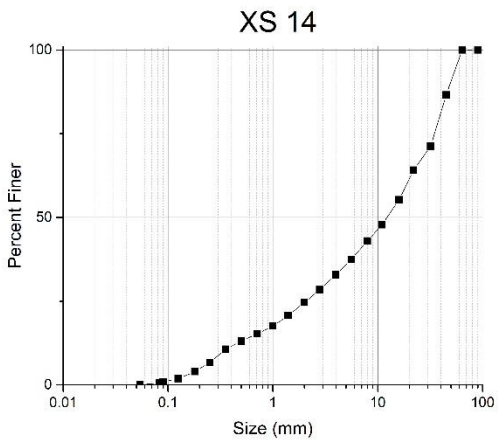
XS 14
Percent Finer
Size (mm)
100
50
0
0.01
0.1
1
10
100

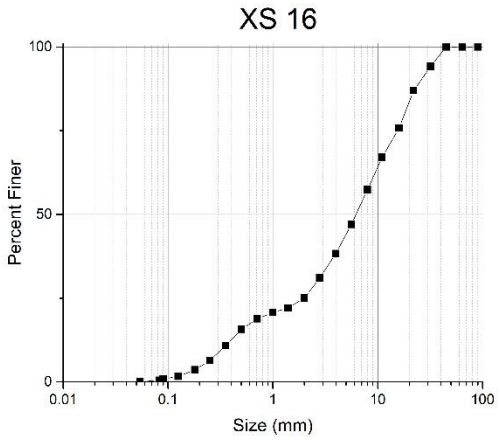
XS 16
Percent Finer
Size (mm)
100
50
0
0.01
0.1
1
10
100

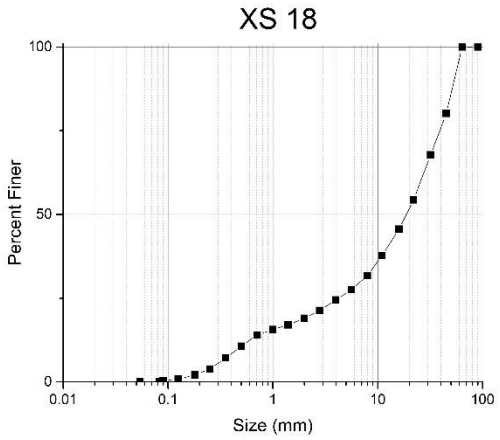
XS 18
Percent Finer
Size (mm)
100
50
0
0.01
0.1
1
10
100

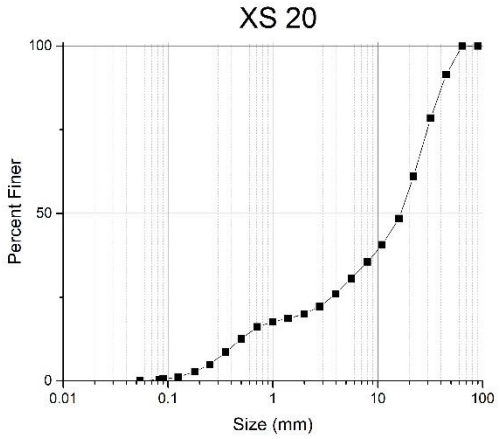
XS 20
Percent Finer
Size (mm)
100
50
0
0.01
0.1
1
10
100

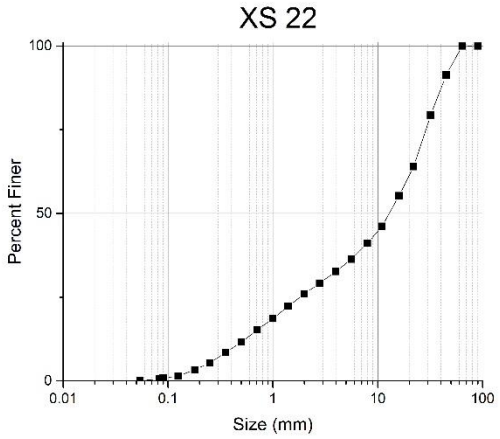
XS 22
Percent Finer
Size (mm)
100
50
0
0.01
0.1
1
10
100

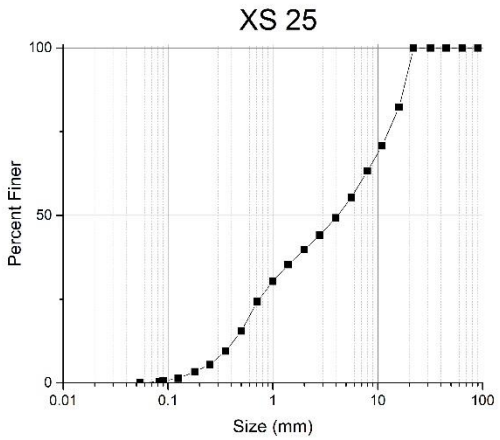
XS 25
Percent Finer
Size (mm)
100
50
0
0.01
0.1
1
10
100

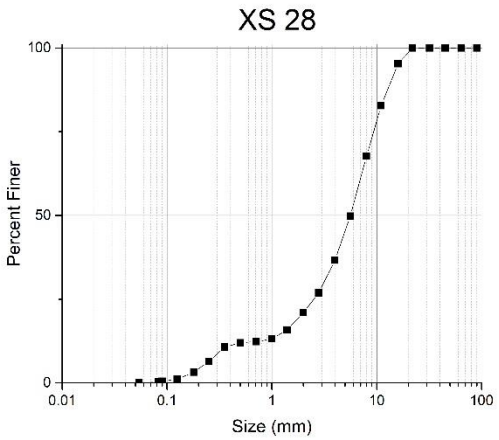
XS 28
Percent Finer
Size (mm)
100
50
0
0.01
0.1
1
10
100

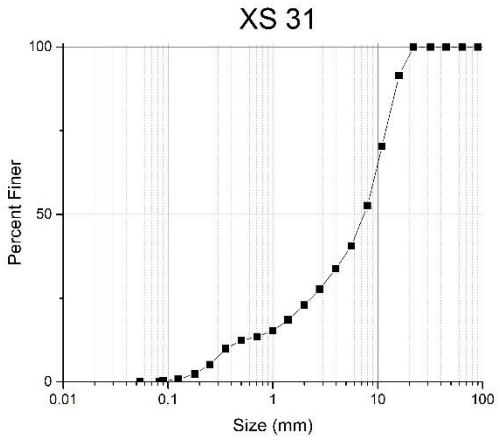
XS 31
Percent Finer
Size (mm)
100
50
0
0.01
0.1
1
10
100

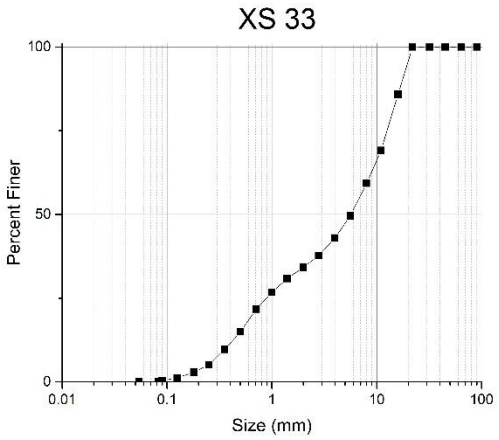
XS 33
Percent Finer
Size (mm)
100
50
0
0.01
0.1
1
10
100

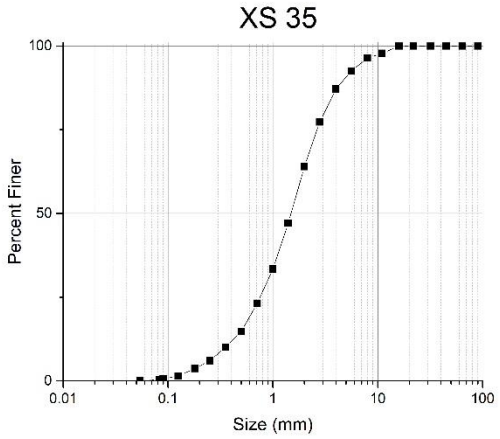
XS 35
Percent Finer
Size (mm)
100
50
0
0.01
0.1
1
10
100

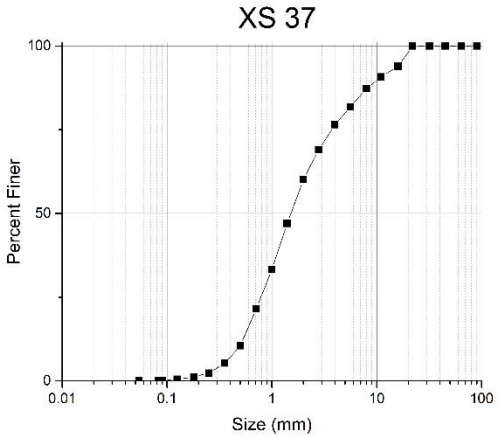
XS 37
Percent Finer
Size (mm)
100
50
0
0.01
0.1
1
10
100

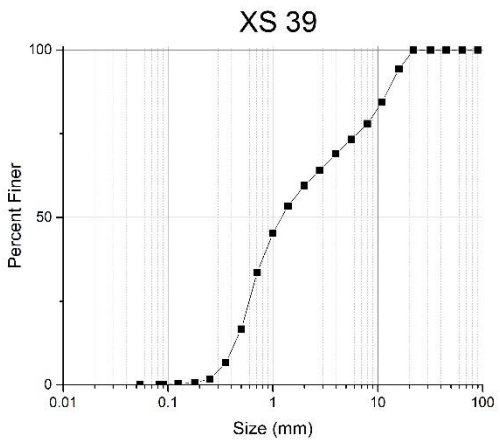
XS 39
Percent Finer
Size (mm)
100
50
0
0.01
0.1
1
10
100

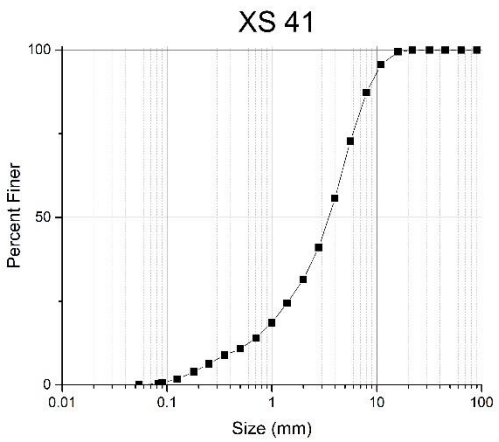
XS 41
Percent Finer
Size (mm)
100
50
0
0.01
0.1
1
10
100

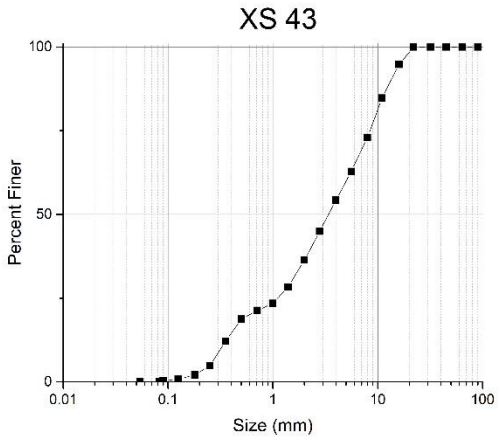
XS 43
Percent Finer
Size (mm)
100
50
0
0.01
0.1
1
10
100

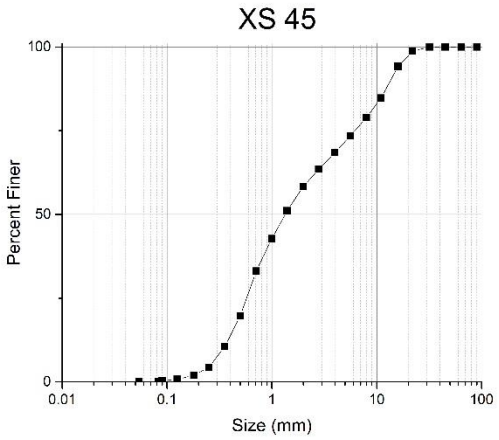
XS 45
Percent Finer
Size (mm)
100
50
0
0.01
0.1
1
10
100

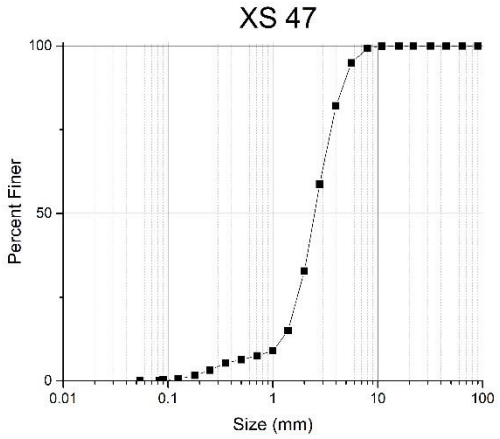
XS 47
Percent Finer
Size (mm)
100
50
0
0.01
0.1
1
10
100

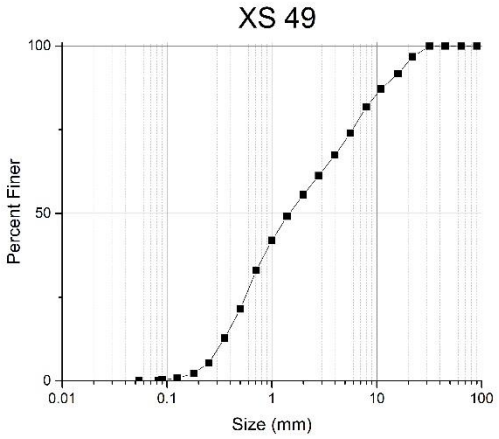
XS 49
Percent Finer
Size (mm)
100
50
0
0.01
0.1
1
10
100

Bed Load Grain Size Distributions

All bed load grain size distributions recorded at FR 1 and FR 2 are shown below. Grey lines are individual bed load measurements. Thick, red lines are the average grain size distribution for bed load.

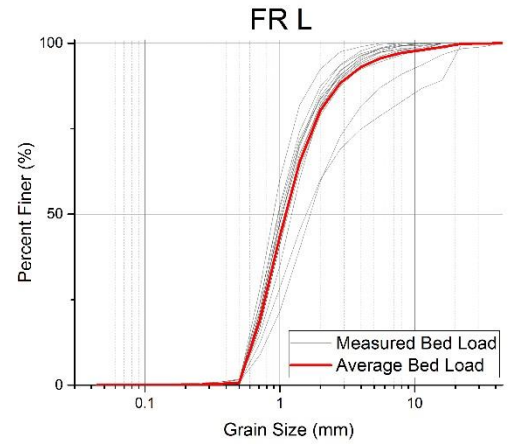

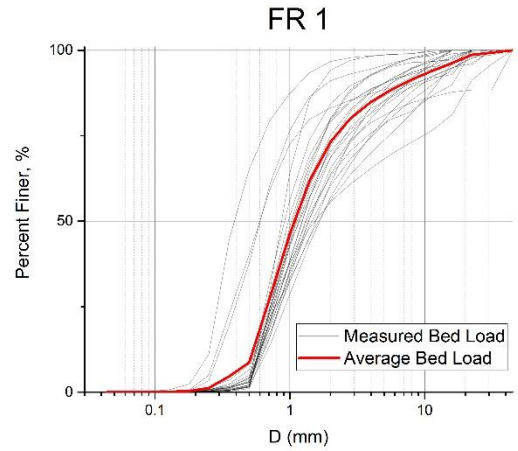

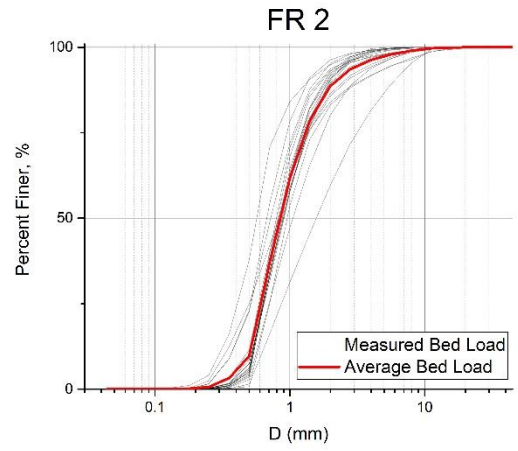

Geomorphic Sediment Budget

Equations for Erosion/Deposition Calculations, where *i* is the cross section where calculations are being performed, *i-1* is the cross section prior to *i*, and *i+1* is the cross section succeeding *i*. Negative values represent erosion; positive values represent deposition.

Erosion/Deposition (m^2):

$$\Delta A_{eros/dep} = \Delta H \times W$$

where $\Delta A_{eros/dep}$ is the cross sectional area change in erosion or deposition. ΔH is the change in depth, and W is the bank-to-bank width.

Erosion/Deposition (m^3):

$$\Delta V_{eros/dep} = \left(\left(\frac{x_{i+1} - x_i}{2}\right) + \left(\frac{x_i - x_{i-1}}{2}\right)\right) \times \Delta A_{eros/dep}$$

where $\Delta V_{eros/dep}$ is the volumetric change in erosion or deposition, *x* is the distance downstream, and *i, i+1, and i-1* refer to a specific cross section.

Erosion/Deposition (kg):

$$Mass\ of\ Erosion = \Delta V_{eros/dep} \times \left(1500 \frac{kg}{m^3}\right)$$

Distance Downstream (m)	Bank-to-Bank Width (m)	Δ Depth (m)	Erosion/ Deposition (m^2)	Erosion/ Deposition (m^3)	Erosion/ Deposition (kg)	Erosion/ Deposition (Mg)
0	8.6	-0.05	-0.40	-22.76	-34100	-34.1
112.56	17.3	-0.02	-0.37	-38.09	-57100	-57.1
206.49	9.0	-0.10	-0.88	-85.01	-127500	-127.5
306.58	16.0	-0.09	-1.44	-136.56	-204800	-204.8
396.48	13.6	-0.11	-1.46	-145.24	-217900	-217.9
506.08	21.0	-0.10	-2.10	-223.54	-335300	-335.3
608.98	14.6	-0.11	-1.64	-171.03	-256500	-256.5
714.32	19.0	-0.11	-2.12	-220.68	-331000	-331.0
817.26	10.0	-0.16	-1.55	-149.60	-224400	-224.4
906.82	11.2	-0.05	-0.52	-49.22	-73800	-73.8
1005.47	11.3	0.09	0.98	101.73	152600	152.6
1114.05	8.1	-0.12	-1.01	-104.04	-156100	-156.1
1212.48	12.0	-0.11	-1.35	-122.80	-184200	-184.2
1296.29	10.0	-0.16	-1.56	-145.26	-217900	-217.9
1399.03	17.0	-0.01	-0.24	-23.00	-34500	-34.5
1491.59	16.0	-0.05	-0.74	-67.81	-101700	-101.7
1582.39	8.3	-0.01	-0.12	-11.70	-17600	-17.6
1687.99	12.0	-0.01	-0.13	-14.68	-22000	-22.0
1809.05	14.9	-0.01	-0.16	-18.25	-27400	-27.4

Distance Downstream (m)	Bank-to-Bank Width (m)	Δ Depth (m)	Erosion/ Deposition (m^2)	Erosion/ Deposition (m^3)	Erosion/ Deposition (kg)	Erosion/ Deposition (Mg)
1911.65	9.5	0.02	0.16	17.19	25800	25.8
2025.02	10.5	-0.00	-0.01	-1.35	-2000	-2.0
2133.62	11.2	-0.01	-0.13	-13.23	-19800	-19.8
2235.39	11.2	-0.03	-0.28	-29.78	-44700	-44.7
2343.14	20.0	0.00	0.05	4.79	7200	7.2
2440.32	10.4	0.00	0.02	2.04	3100	3.1
2534.89	9.5	0.02	0.17	17.30	25900	25.9
2639.41	11.0	-0.05	-0.49	-49.56	-74300	-74.3
2736.18	12.0	0.01	0.13	13.22	19800	19.8
2849.03	15.5	-0.06	-0.98	-99.77	-149700	-149.7
2940.16	15.0	0.04	0.66	72.02	108000	108.0
3065.8	11.4	-0.06	-0.73	-83.02	-124500	-124.5
3166.62	8.6	-0.03	-0.40	-36.11	-54200	-54.2
3248.23	17.3	-0.04	-0.61	-68.70	-103000	-103.0
3391.16	9.0	-0.03	-0.43	-49.89	-74800	-74.8
3481.09	16.0	-0.10	-1.47	-232.77	-349200	-349.3
3708.71	13.0	-0.10	-1.34	-224.28	-336400	-336.4
3816.23	10.3	-0.03	-0.32	-33.46	-50200	-50.2
3919.87	14.0	-0.14	-1.93	-214.21	-321300	-321.3
4037.84	10.5	-0.09	-0.89	-92.20	-138300	-138.3
4127.09	11.0	-0.04	-0.46	-44.77	-67200	-67.2
4234.51	13.5	-0.07	-0.95	-147.04	-220600	-220.6
4438.33	12.1	-0.04	-0.43	-64.89	-97300	-97.3
4539.02	11.6	0.06	0.75	68.56	102800	102.8
4622.16	8.7	0.02	0.15	14.77	22200	22.2
4732.98	11.3	-0.06	-0.63	-75.31	-113000	-113.0
4861.4	10.5	-0.05	-0.51	-60.81	-91200	-91.2
4971.3	14.5	-0.05	-0.76	-89.14	-133700	-133.7
5095.96	17.7	-0.03	-0.60	-37.22	-55800	-55.8
Total Erosion/Deposition (kg or Mg) from XS 0 to FR 1:					-2302600	-2303
Total Erosion/Deposition (kg or Mg) from FR 1 to FR 2:					-2475100	-2475